Experimental Neurology 387 (2025) 115186

Contents lists available at ScienceDirect

Experimental Neurology

journal homepage: www.elsevier.com/locate/yexnr

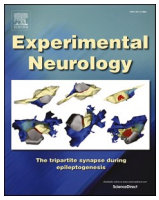

Research paper

Partial microglial depletion through inhibition of colony-stimulating factor 1 receptor improves synaptic plasticity and cognitive performance in aged mice

Luisa Strackeljan [a], David Baidoe-Ansah [a], Hadi Mirzapourdelavar [a], Shaobo Jia [a], Rahul Kaushik [a], Carla Cangalaya [a], Alexander Dityatev [a,b,c,*]

[a] Molecular Neuroplasticity, German Center for Neurodegenerative Diseases (DZNE), Magdeburg, Germany
[b] Center for Behavioral Brain Sciences (CBBS), 39106 Magdeburg, Germany
[c] Medical Faculty, Otto-von-Guericke University, 39120 Magdeburg, Germany

ARTICLE INFO

Keywords:
Aging
Glia
Extracellular matrix
Synapses
Parvalbumin
Brevican
Perineuronal nets
Perisynaptic ECM

ABSTRACT

Microglia depletion, followed by repopulation, improves cognitive functions in the aged mouse brain. However, even temporal ablation of microglia puts the brain at a high risk of infection. Hence, in the present work, we studied if the partial reduction of microglia with PLX3397 (pexidartinib), an inhibitor of the colony-stimulating factor 1 receptor (CSF1R), could bring similar benefits as reported for microglia ablation. Aged (two-years-old) mice were treated with PLX3397 for a total of 6 weeks, which reduced microglia numbers in the hippocampus and retrosplenial cortex (RSC) to the levels seen in young mice and resulted in layer-specific ablation in the expression of microglial complement protein C1q mediating synaptic remodeling. This treatment boosted long-term potentiation in the CA1 region and improved performance in the hippocampus-dependent novel object location recognition task. Although PLX3397 treatment did not alter the number or total intensity of *Wisteria floribunda* agglutinin-positive perineuronal nets (PNNs) in the CA1 region of the hippocampus, it changed the fine structure of PNNs. It also elevated the expression of perisynaptic proteoglycan brevican, presynaptic vGluT1 at excitatory synapses, and vGAT in inhibitory ones in the CA1 *stratum radiatum*. Thus, targeting the CSF1R may provide a safe and efficient strategy to boost synaptic and cognitive functions in the aged brain.

1. Introduction

Brain aging and its underlying molecular and cellular processes have gained continuous attention over the last few decades. In various brain regions, aging is accompanied by a decline in neural resources, resulting in impairment of learning and memory. In the hippocampus, aging is associated with a loss of neurons (Fu et al., 2015), impaired neurogenesis in the dentate gyrus (Gil-Mohapel et al., 2013; Ben Abdallah et al., 2010), and alterations in dendrites and synaptic transmission (Rosenzweig and Barnes, 2003; Ianov et al., 2017; Bohlen und Halbach O von, Zacher C, Gass P, Unsicker K., 2006) (Bettio et al., 2017). Functionally, it is connected to cognitive decline (Shors et al., 2001; Deng et al., 2010), as exemplified by a recent study of 20-month-old mice showing difficulties in different behavioral paradigms, including object recognition and spatial navigation tasks linked to the hippocampal function (Yang et al., 2021).

An essential characteristic of brain aging is the increasing low-grade neuroinflammation, the so-called “inflammaging” (von Bernhardi et al., 2015). Activation of the cGAS-STING signaling by cytosolic DNA released from perturbed mitochondria in old microglia is a critical driver of microglia activation during aging (Gulen et al., 2023). It manifests in a shift in cytokine balance towards higher levels of pro- and reduction in anti-inflammatory cytokines and impaired cognitive flexibility and stress responses in humans and animals (Sparkman and Johnson, 2008).

Abbreviations: CSF1R, Colony-stimulating factor 1 receptor; CSPG, Chondroitin sulfate proteoglycan; DG, Dentate gyrus; ECM, Extracellular matrix; fEPSP, Excitatory postsynaptic potential; NOLT, Novel object location task; NORT, Novel object recognition task; PB, Phosphate buffer; PBS, Phosphate-buffered saline; PFA, Paraformaldehyde; PNN, Perineuronal net; PPF, Paired-pulse facilitation; PPR, Paired-pulse ratio; PV, Parvalbumin; OLG, Oligodendrocyte; RSC, Retrosplenial cortex; RT, Room temperature; SEM, Standard error of mean; TBS, Theta-burst stimulation; WFA, *Wisteria floribunda* agglutinin.

* Corresponding author at: Molecular Neuroplasticity, German Center for Neurodegenerative Diseases (DZNE), Magdeburg, Germany
E-mail address: alexander.dityatev@dzne.de (A. Dityatev).

https://doi.org/10.1016/j.expneurol.2025.115186
Received 13 November 2024; Received in revised form 4 February 2025; Accepted 12 February 2025
Available online 14 February 2025

Aging also changes the morphology of microglia, the brain's innate immune cells, towards a more amoeboid phenotype associated with activation upon injury or inflammation. The cell body increases in size while the normally lengthy and versatile processes shorten and thicken (Damani et al., 2011). Secondly, the motility and the ability to react to injury and phagocytize cellular debris are decreased. Finally, microglia lose their ability to proliferate. This cellular senescence is typical for various aging brain cells (Sikora et al., 2021) and leads to increased iron storage, ferritin overexpression, and elevated release of neurotoxic molecules (Angelova and Brown, 2019).

Pharmacological depletion of microglia by CSF1R inhibitors has gained attention, as this approach allows one to rather specifically study the effects of microglia reduction at any time point within the lifespan of mice (Elmore et al., 2014). It has been shown that microglia repopulation after withdrawal of the CSF1R inhibitor resulted in improved spatial memory function in the Morris water maze in aged animals and rescue of age-related deficits in the long-term potentiation (LTP) following theta-burst stimulation to Schaffer collateral-commissural projections (Elmore et al., 2018).

Microglia secrete extracellular matrix (ECM) molecules as well as extracellular proteases, and these mechanisms are altered with age and in age-associated pathologies. Functionally, attenuation of ECM can either promote or inhibit synaptic plasticity (Dityatev et al., 2010). For example, mice deficient in the ECM glycoprotein tenascin-R, chondroitin sulfate proteoglycans (CSPGs) brevican or versican, or treated with chondroitinase ABC to digest chondroitin sulfates display impaired LTP in the CA1 (Brakebusch et al., 2002; Chelini et al., 2024). On the other hand, a study by Vegh and colleagues has shown that perisynaptic ECM proteins, including brevican, are progressively upregulated with aging, both on genetic and proteomic levels, coinciding with an impairment of hippocampus-dependent spatial memory (Végh et al., 2014). Furthermore, attenuation of ECM with chondroitinase ABC reversed the age-dependent cognitive deficits in motor learning (Richard et al., 2018). These data indicate that the optimal levels of ECM support the synaptic plasticity, but excessive loss or accumulation of ECM results in impaired LTP and learning.

Several studies have shown an interaction between microglia and the brain ECM in young and aged mice (Crapser et al., 2020; Nguyen et al., 2020). For example, a gene expression analysis showed that long-term depletion of microglia enhances the mRNA levels of *brevican* in the hippocampus of wild-type mice (Spangenberg et al., 2019), and we recently confirmed this increase at a protein level using immunohistochemistry in young adult mice (Strackeljan et al., 2021). Microglia remodeling of ECM enhances synaptic plasticity by engulfing and remodeling ECM, especially at synapses, which is essential for long-term memory consolidation (Nguyen et al., 2020). However, this concept of microglia and ECM interaction has not been fully explored regarding age-dependency, although both microglia senescence and hippocampal perisynaptic ECM were reported to increase with age (Végh et al., 2014; Tremblay et al., 2012).

Here, we aimed to study whether modest inhibition of CSF1R could reverse age-related deficits in the mouse brain and what mechanisms might be underlying the rescue. Using the CSF1R-inhibitor PLX3397, we reduced microglia numbers to the level seen in young mice and found increased LTP in the CA1 region and cognitive improvement in the novel object location recognition task. These changes were associated with reduced phagocytic cues produced and secreted by microglia.

2. Materials and methods

2.1. Animals

Twenty male C57BL6J mice aged between 24 and 26 months were used in this study. During the experimentation period, four animals (3 controls and 1 PLX-treated) died and were not part of further experiments. Animals were housed individually under standard conditions, including *ad libitum* access to food and water and a 12-h light/12-h dark cycle. All animal experiments were conducted in accordance with the ethical animal research standards defined by German law and the recommendations of the Ethical Committee on Animal Health and Care of the State of Saxony-Anhalt, Germany (license number: 42502–2-1346).

2.2. PLX3397 treatment

The animals were treated with the CSF1R inhibitor PLX3397 (pexidartinib; MedChemExpress). The drug was mixed into the animal chow at a nominal concentration of 290 mg/kg (ssniff Spezialdiäten GmbH; Elmore et al., 2014). The mice received fresh control (product number 1534–70) or PLX-chow daily, and their food intake was recorded. On average, mice consumed 5 g of chow daily with no significant difference between groups. The treatment started 28 days before the first behavioral testing. Mice were fed with PLX3397 for 6 weeks before being sacrificed and studied electrophysiologically and immunohistochemically (see timeline, Fig. 1).

2.3. Behavior

2.3.1. Behavioral analysis

To study different forms of memory, we performed behavioral tests, including the novel object location task (NOLT), the novel object recognition task (NORT), and the labyrinth task (dry maze). All behavioral tests were video-recorded and the animal's performance was analyzed using Anymaze 4.99 (Stoelting Co., Wood Dale, IL, USA).

2.3.2. Open field

To study locomotor activity and anxiety-associated behavior, the mice were put into an open field arena (50 × 50 × 30 cm) (Hölter et al., 2015; Kaushik et al., 2018) and studied using an overhead camera for 10 min. The arena was virtually divided into a central area (30 × 30 cm) and a peripheral region (the 10 cm area adjacent to the wall of the recording chamber). The overall physical and emotional state of mice was determined using the total distance moved and time spent in both the central and peripheral areas.

2.3.3. Novel object location test

The novel object location test was carried out as previously described (Baidoe-Ansah et al., 2022), including the encoding and retrieval phases (Vogel and Marcotte, 2012). The encoding phase lasted 10 min, during which mice were allowed to explore two indistinguishable objects. During the 10-min retrieval phase, which was carried out 24 h later, one of the objects was repositioned to a novel position. To analyze the animal's behavior, the exploration times for an object located at familiar (F) and novel (N) positions, as well as the discrimination ratio [(N—F)/(N + F)] x 100 % were used.

2.3.4. Novel object discrimination test

The novel object recognition test was also conducted in the open-field arena, including the encoding and retrieval phases described previously (Baidoe-Ansah et al., 2022; Antunes and Biala, 2012). Briefly, the animals were allowed to explore the arena with two identical objects for 10 min. After 24 h, one of the objects was replaced by a novel one, and the exploration time was measured again. Exploration time for familiar (F) and novel (N) objects, as well as the discrimination ratio [(N—F)/(N + F)] x 100 %, were used to evaluate animals' recognition memory.

2.3.5. Labyrinth task (dry maze)

A quadrant-based labyrinth task was designed to measure hippocampus-dependent spatial learning and memory in aged mice. This task was designed and implemented as an alternative to the Morris water maze (MWM) task that uses imaginary quadrants (software) compared to actual quadrants. Comparatively, this task is less stressful

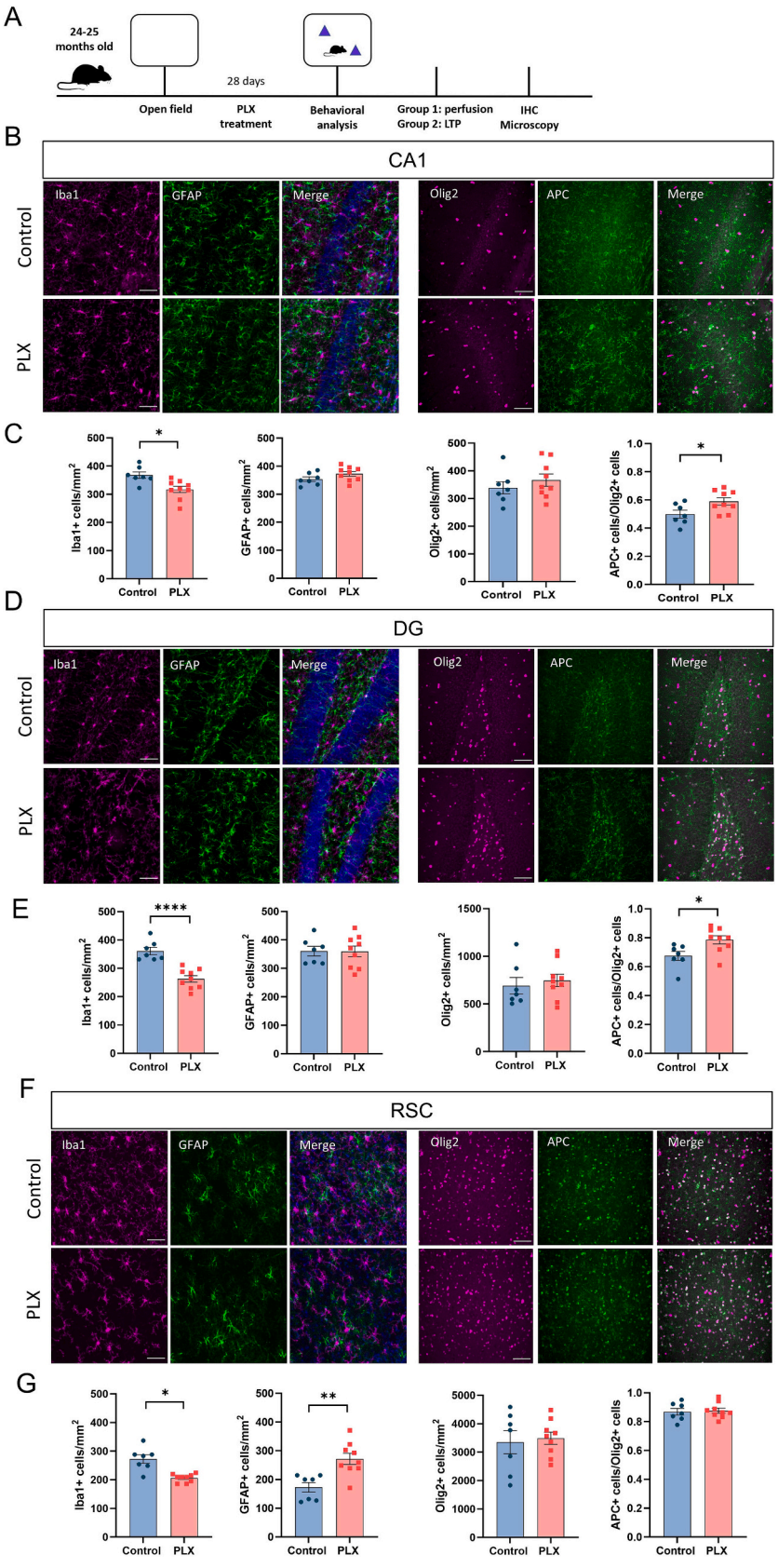

(caption on next page)

Fig. 1. PLX treatment reduces microglia density and affects oligodendrocyte maturation and astrocytic actvation in a region-specific manner. (A) Timeline of the experiment. (B) 20× representative images of glial cells in the hippocampal CA1, (D) dentate gyrus (DG) and (F) retrosplenial cortex (RSC). Microglia (Iba1, left panel, magenta), astrocytes (GFAP, left panel, green), oligodendrocytes (Olig2, right panel, magenta) and APC+/Olig2+ cells (APC, right panel, green). (C) PLX treatment reduces microglia density in the CA1. The density of oligodendrocytes and the proportion of APC+/Olig2+ cells are not changed. (E) In the DG, the findings are similar to those in the CA1. (G) In the RSC, Iba1+ cell density is decreased while the density of GFAP+ cells is increased. There is no change in oligodendrocytes. Scale bar, 50 μm. Bar graphs show mean ± SEM values. *$p < 0.05$, ** $p < 0.01$, ****$p < 0.0001$; *t*-test, $n = 6$–9 mice per group. (For interpretation of the references to colour in this figure legend, the reader is referred to the web version of this article.)

and capable of distinguishing between navigational strategies used by mice, namely egocentric (route) and allocentric (place) (Rich and Shapiro, 2007; Harrison and Feldman, 2009).

The labyrinth was designed with four entry points in four quadrants of equal size but with different intra-quadrant configurations. In each quadrant configuration, zones were defined to quantify errors (with pink highlights). As outlined above, the asymmetrical-quadrant-based labyrinth was carried out with distal cues placed on curtains to enclose the maze and reward (water) placed in the 4th quadrant. Two entry paths (start1 and 2) were used for all daily training sessions from day 1 (D1) to day 3 (D3), and a different path was used for probe tests (Probe Trial). On D1, mice were allowed to explore the maze for 10 min with reward. Subsequent training sessions, two trials per day for 2 days (D2 & D3), were ended upon entry into the reward zone. An inter-trial delay of 1 h was implemented for each daily training session. With the probe test, mice entered the maze through the probe entry path, and the session was manually ended upon entry into the reward zone. Using an overhead camera with animal tracking software (Anymaze 4.99: Stoelting Co., Wood Dale, IL, USA), parameters such as the distance traveled, errors made and latency to the reward were recorded and quantified.

2.4. Electrophysiology

Four randomly chosen animals from each group were used for electrophysiological analysis. Animals were deeply anesthetized with isoflurane and perfused transcardially with ice-cold sucrose-based cutting solution containing (in mM): 230 sucrose, 2 KCl, 1 $MgCl_2$, 2 $MgSO_4$, 1.25 NaH_2PO_4, 26 $NaHCO_3$, 1 $CaCl_2$ and 10 D-Glucose, then decapitated. Hippocampi were isolated and placed on an agar block to cut transverse slices (350 μm thick) using a vibrating microtome (VT1200S, Leica). Slices were transferred and incubated in a submerged chamber with a solution containing (in mM): 113 NaCl, 2.38 KCl, 1.24 $MgSO_4$, 0.95 NaH_2PO_4, 24.9 $NaHCO_3$, 1 $CaCl_2$, 1.6 $MgCl_2$, 27.8 D-glucose for at least 2 h at room temperature. Next, the slices were transferred to the recording chamber and were continuously perfused with the solution containing (in mM) 120 NaCl, 2.5 KCl, 1.5 $MgCl_2$, 1.25 NaH_2PO_4, 24 $NaHCO_3$, 2 $CaCl_2$ and 25 D-Glucose. All solutions were saturated with 95 % O_2 and 5 % CO_2 and the osmolality was adjusted to 300 ± 5 mOsm. Thin glass electrodes filled with ACSF were used for stimulation and recording of fEPSPs. The CA3-CA1 pathway was stimulated two times by the theta-burst stimulation (TBS) trains to induce LTP. The stimulation intensity was determined based on the input-output curve. It was set to give fEPSPs with a slope of ~30 % and ~ 50 % of the supramaximal fEPSP for the paired-pulse facilitation (PPF) and LTP induction, respectively. Single stimuli were repeated every 20 s for at least 10 min for baseline recording before and for 60 min after LTP induction. The paired-pulse ratio (PPR) was evaluated at different time intervals under the same conditions. All recordings were obtained at room temperature using an EPC-10 amplifier (HEKA Elektronik). The recordings were digitized at 10–20 kHz and filtered at 1–3 kHz.

2.5. Tissue preparation

For tissue preparation, animals were anesthetized with isoflurane and then transcardially perfused with PBS, followed by 4 % paraformaldehyde (PFA). Brains were dissected and fixed in 4 % PFA in phosphate-buffered saline (PBS) overnight at 4 °C. Afterwards, the tissue was transferred to 30 % sucrose in PBS for two nights before being frozen in methylbutane at −80 °C. Using a cryostat at −20 °C coronal brain sections of 40-μm thickness were prepared and stored in a cryoprotectant solution (ethylene glycol based; 30 % ethylene glycol, 30 % glycerol, 10 % 0.2 M sodium phosphate buffer pH 7.4, in dH2O) at 4 °C.

2.6. Immunohistochemistry

Immunohistochemistry (IHC) was performed based on our previous protocol (Strackeljan et al., 2021). In short, all sections were washed 3 times with 120 mM phosphate buffer (PB), pH = 7.2 for 10 min at room temperature (RT), followed by permeabilization with 0.5 % Triton X-100 (Sigma T9284) in phosphate buffer for 10 min and blocking in PB supplemented with 0.1 % Triton X-100 and 5 % normal goat serum (Gibco 16,210–064) for 1 h at RT. For primary antibody delivery, the sections were incubated for 20 h at 37 °C (see Table 1). After washing in PB, sections were incubated with conjugated secondary antibodies for 90 min at RT. Labeled sections were rewashed, mounted, and coverslipped on glass slides using Fluoromount medium (Sigma; Cat no. F4680).

2.7. Confocal microscopy and image processing

Images were acquired using a Zeiss confocal microscope (LSM 700).

Table 1
Primary and secondary antibodies used for IHC.

Primary reagents	Supplier, product number	Dilution
Chicken anti-PV	Synaptic Systems, 195 006	1:500
Rabbit anti-Brevican	(Seidenbecher et al., 1995; John et al., 2006)	1:1000
Guinea pig anti-Iba1	Synaptic Systems, 234 004	1:500
Guinea pig anti-vGluT1	Synaptic Systems, 235 304	1:1500
Chicken anti-GFAP	Sigma Aldrich, AB5541	1:400
Rabbit anti-Olig2	Sigma Aldrich, AB9610	1:200
Mouse anti-APC	Merck Millipore, OP80-100UG	1:500
Rabbit anti-C1q	Abcam, AB182451	1:500
Rat anti-CD68	AbD Serotec, MCA1957	1:500
Biotinylated WFA	Vector Laboratories, B-1355	1:1000
Rabbit anti-vGAT	Synaptic Systems, 131 002	1:500
Mouse anti-PSD95	Abcam, ab2723	1:500
Sheep anti-Neurocan	R&D Systems, AF5800	1:20
Rabbit anti-Aggrecan	Millipore, AB1031	1:200
Secondary reagents	**Supplier**	**Dilution**
Alexa Fluor 405 goat Anti-Chicken IgG	Abcam, ab175675	1:500
Alexa Fluor 647 goat Anti-Chicken IgG	Invitrogen, A21449	1:1000
Alexa Fluor 647 goat Anti-Rabbit IgG	Invitrogen, S32351	1:1000
Alexa Fluor 405 donkey Anti-Guinea pig IgG	Sigma Aldrich, SAB4600230	1:500
Alexa Fluor 647 goat Anti-Mouse IgG	Invitrogen, A21236	1:1000
Alexa Fluor 488 goat Anti-Guinea pig IgG	Invitrogen, A21044	1:1000
Alexa Fluor 546 goat Anti-Rabbit IgG	Invitrogen, A11035	1:500
Alexa Fluor 546 donkey Anti-Sheep IgG	Invitrogen, A21098	1:500
Streptavidin Alexa Fluor 405 conjugated	Invitrogen, S32351	1:1000

Brain regions were determined following the Allen mouse brain atlas. All images were further processed and analyzed using the open software ImageJ (Fiji) version 1.54 f.

2.8. Glial cell counting and microglia analysis

Counting of microglia, astrocytes, and oligodendrocytes. Images were acquired at 20× objective for hippocampal CA1, CA2, and CA3 areas, the dentate gyrus (DG) and the retrosplenial cortex (RSC). Glial cells were then counted using the Cell Counter plug-in in Fiji. Two markers were used to analyze the oligodendrocytes (OLGs): Olig2, which labels all OLGs, and APC, expressed in astrocytes and OLGs. In the latter, APC is known to label myelinating mature OLGs specifically. We then calculated the percentage of APC+/Olig2+ cells in one ROI.

Morphological analysis of microglia cells. For the morphological analysis of microglia cells, images were acquired using a 40× objective for hippocampal CA1. A similar protocol was used to one published elsewhere (Green et al., 2022). For each mouse, three images were used for further analysis. In total, $n = 71$ microglia from 6 control mice and 100 microglia from 9 PLX-treated mice were analyzed.

Image pre-processing. In brief, the brightness/contrast was automatically adjusted in Fiji to visualize best the branches of the microglia (Fig. S2A). The unsharp mask (radius = 3, mask = 0.60) was then applied to increase the contrast of the image further, and the "remove outliers" function (radius = 2, threshold = 50) was applied to remove noisy pixels. Two microglia cells with entire soma visible through *Z*-stack were selected for maximum intensity projection from each image (Fig. S2B). The threshold was then automatically adjusted using the Otsu's method. The paintbrush tool was used to connect any branches that became fragmented due to image processing, using the original photomicrograph as a reference. After binarization, the "close" function in the binary image processing kit was applied; then any fragments that were not attached to the cell and noise pixels were detected with "analyze particles" function (size: 0–100 μm^2) and excluded from further analysis (Fig. S2C).

Skeletal analysis. The binarized single-cell images were skeletonized (Fig. S2D) for the skeletal analysis. Branches per microglia, junctions per microglia, endpoints per microglia, averaged branch length and maximum branch length were calculated per cell using the "Analyze skeleton" Fiji function.

Fractal analysis. The same binary images were converted into outlines (Fig. S2E). The FracLac plug-in was used to analyze the cells, with 'box-counting' applied and the 'grid design Num G'set to 4. The convex hull and bounding circle of the cell were measured. The fractal dimension (Db, a statistical measure of pattern complexity), lacunarity (a geometric measure of how a pattern fills space), circularity (how circular the microglial cell is), span ratio (longest length/longest width), and density (number of pixels/area) were measured.

Sholl analysis. The same binary images were used for the Sholl analysis. The center of the cell body was selected with a point-tool. For concentric circle placement, the radius was set from 4 to 50 μm; the distance between each circle was 2 μm for all cells. The number of times that the microglial branches intercepted each of the circles, the total number of intersections, the critical radius (at the circle with the largest number of interceptions), and the Sholl decay index (also known as Sholl regression coefficient, the slope of decay of the intersection-number with distance from the center of analysis) were calculated.

2.9. Analysis of PNNs around PV+ cells and perisynaptic ECM

Parvalbumin-positive cells (PV+ cells) and their surrounding PNNs were counted using the Cell Counter in Fiji. Biotinylated *Wisteria floribunda agglutinin (WFA)* was used to label the ECM of perineuronal nets (PNN). Furthermore, we used antibodies against various PNN components such as aggrecan, brevican, and neurocan and measured the ECM mean intensity around PV+ cells.

The single PNN units were analyzed using APNU 2.0 as described previously (Strackeljan et al., 2021; Kaushik et al., 2021). In short, this semi-automatic algorithm outlines PNN holes and measures hole-surrounding ECM in the area limited by local peaks in the ECM expression. The results table then contains various key characteristics of PNN units, such as size, density, and circularity in 2D and 3D. To ensure a seamless analysis of the PNN fine structure, a z-stack of 40 images with an interval of 0.1 μm was collected per PNN using a 63× objective. A Fiji plug-in for PNN unit analysis is available at https://data.mendeley.com/datasets/cvf924fz3p/1.

For analysis of perisynaptic ECM molecules, we used a customized Fiji plug-in that specifically measured perisynaptic brevican around single presynaptic puncta.

2.10. Analysis of inflammatory markers

To study the effect of microglia reduction on neuroinflammation and phagocytosis, we used IHC to stain for C1q, CD68, and TREM2. For C1q and TREM2, global mean intensity was measured (Benetatos et al., 2020). For CD68, we only analyzed particles inside microglia cell bodies by outlining the cell soma and measuring a signal inside the ROIs.

2.11. Statistical analysis

All bar graphs are expressed as the mean ± standard error of the mean (SEM). Statistical analysis was performed using GraphPad Prism 8.0 (GraphPad Software Inc., La Jolla, CA, USA) and XLSTAT software (Addinsoft Inc., N.Y., USA). Gaussian distribution of the data was verified using the Kolmogorov-Smirnov, Shapiro-Wilk, or D'Agostino tests. Unless otherwise stated, pairwise comparisons of parameters were performed after averaging per animal using a two-tailed Student's *t*-test for Gaussian distributions; the Mann-Whitney test was employed if the data did not follow the Gaussian law. Comparison of vGlut1 expression between groups was done using the one-tailed t-test for the alternative hypothesis that the intensity is higher in the PLX-treated than in control mice because our previous study revealed an increase in the intensity of vGluT1 puncta (Strackeljan et al., 2021).

For PNN unit analysis and expression of cellular and synaptic markers, the Kolmogorov-Smirnov test was employed for between-group comparison of cumulative frequency distribution functions of individual cellular/synaptic values in addition to the analysis of mean values per animal. Statistical significance was set at $p < 0.05$.

3. Results

3.1. PLX treatment reduces microglia density

Oral administration of the CSF1R inhibitor PLX3397 (pexidartineb) in two-year-old mice for 6 weeks led to a partial reduction in microglia in the hippocampus and retrosplenial cortex (RSC). Using two-way RM ANOVA, we observed that PLX treatment accounted for about 30 % of the total variance observed ($p < 0.0001$), while the brain region identity (hippocampal CA1, DG, or RSC) accounted for 44 % ($p < 0.0001$). We then performed post hoc tests to evaluate the PLX effects for each region and revealed a microglia reduction by 14 % in the CA1 (Fig.1B, C; 368.1 ± 11.2 vs. 317.2 ± 11.3 cells/mm^2, *t-test* with the Bonferroni correction for multiple comparisons here and below, $p = 0.021$), by 27 % in the dentate gyrus (Fig.1D, E; 361.1 ± 13.1 vs. 263.0 ± 11.7 cells/mm^2, *t-test*, $p < 0.0003$) and by 25 % in the RSC (Fig. 1F, G; 272.6 ± 15.08 vs. 206.1 ± 4.72 cells/mm^2, *Wel's t-test*, $p = 0.0114$). As aging increases microglia numbers (Vaughan and Peters, 1974), we included a group of 3-month-old mice to compare microglia in young and aged mice. After the PLX treatment, the density of microglia in the CA1 region of aged animals was equal to that of young controls (Fig. S1).

3.2. Effects of PLX treatment on other glial cells

In young animals, PLX administration is specific to microglia and does not change the number of other glial cells (Elmore et al., 2014). To explore this aspect in aged animals, we used GFAP as an astrocytic marker. We could not detect any differences in GFAP+ cell number in the hippocampal CA1 or DG, but in the RSC, the microglia reduction was accompanied by increased GFAP+ cell numbers (Fig. 1F, G; 173.0 ± 16.5 vs. 271.8 ± 19.3 cells/mm^2, *U test*, $p = 0.0051$). Using antibodies against the transcription factor Olig2, which is expressed in oligodendrocytes (OLGs) and labels OLGs at all developmental stages (Takebayashi et al., 2000), and APC (adenomatous polyposis coli) that is crucial for oligodendrocyte differentiation and myelination (Lang et al., 2013), we explored changes in OLG density. We did not detect differences in the overall Olig2+ cell number or the proportion of APC+/Olig2+ oligodendrocytes, suggesting normal myelination after the PLX treatment in aged mice.

3.3. Morphological changes in microglia and characteristics of cell senescence

To further characterize the morphology and the state of microglia, we focused on the CA1 region of the hippocampus as PLX treatment abrogated aging-associated decline in CA1 LTP and this region is highly involved in the novel object location task, performance in which was also improved by PLX treatment, as shown below (sections 3.4 and 3.5). PLX treatment slightly increased the Iba1 intensity in the remaining microglia (Fig. 2B,C; 1.0 ± 0.01 vs. 1.14 ± 0.06, *U test*, $p = 0.0076$). No difference, however, was found in the area of microglial soma (Fig. 2C; 240.1 ± 3.6 μm^2 vs. 239.7 ± 4.4 μm^2, *KS-test*, $p = 0.62$), suggesting no major microglia activation by PLX treatment.

Further, we performed skeletal analysis, fractal analysis and Sholl analysis of microglia morphology. Single-cell skeletal analysis was used to quantify microglial ramification. The only difference detected was in the maximal branch length, which was reduced in PLX-treated mice (Fig. S2K, 13.450 ± 0.723 μm vs. 11.500 ± 0.357 μm; *t*-test, $p = 0.023$). There was no statistical difference between control group and PLX-treated group on other parameters extracted by the skeletal analysis (Fig. S2G-J), such as the number of branches per microglia (263.7 ± 20.0 vs. 265.5 ± 15.3); junctions per microglia (125.9 ± 9.9 vs. 126.8 ± 7.3); endpoints per microglia (129.4 ± 8.7 vs. 130.1 ± 7.0); and average branch length (2.37 ± 0.04 μm vs. 2.39 ± 0.05 μm). Fractal analysis was used to quantify the spatial complexity of the individual microglia. No significant difference between control group and PLX-treated group was revealed using this method (Suppl. Fig. S2L—P) in the fractal dimension (1.517 ± 0.013 vs. 1.523 ± 0.006); lacunarity (0.362 ± 0.007 vs. 0.357 ± 0.005); circularity (0.848 ± 0.011 vs. 0.837 ± 0.009); span ratio (1.437 ± 0.060 vs. 1.455 ± 0.043); and density (0.080 ± 0.004 vs. 0.076 ± 0.002). The Sholl analysis was applied to determine the extent of branching as a function of the distance from the soma. No significant differences were detected in the distribution of intersections along distance (Fig. S2Q, $P_{treatment} = 0.812$, two-way RM ANOVA) as well as other parameters (Fig. S2R-T): total intersections (155.3 ± 8.7 vs. 147.2 ± 2.4); critical radius (17.63 ± 0.45 vs. 17.39 ± 0.78 μm); and the Sholl decay index (0.147 ± 0.007 vs. 0.144 ± 0.004). In conclusion, PLX treatment primarily does not influence the morphology of microglia at the single-cell level.

It has been reported that the microglia that repopulate the brain after PLX5622 treatment show similar characteristics to young cells, i.e. there is a change in the senescent state of microglia (Elmore et al., 2018). Hence, we performed an immunohistochemical analysis for ferritin storage and lipofuscin aggregates as biomarkers for cellular senescence. The mean intensity of ferritin inside Iba1+ cells per animal was not significantly changed in PLX-treated animals (1 ± 0.09 vs. 1.2 ± 0.1; *t*-test, $p = 0.18$), but studying the cumulative frequency distribution of single Iba1+ cells we observed a shift to the right indicative of higher level of Ferritin signal after PLX treatment (*KS-test*, $p = 0.0003$). Likewise, the intensity of the lipofuscin autofluorescence inside microglia cell bodies was higher in the remaining microglia in the PLX-treated group (1 ± 0.01 vs. 1.18 ± 0.06; *Welsh's t-test*, $p = 0.027$; *KS-test*, $p = 0.025$). This finding suggests that PLX treatment in our conditions did not reduce the number of senescent microglia and even slightly promoted the senescent state.

3.4. PLX treatment improves performance in novel object location test in aged animals

It is known that aging leads to hippocampus-dependent learning deficits in humans and mice (Végh et al., 2014). To test for hippocampal-dependent learning and memory, we performed behavioral tests during 2 weeks following 4 weeks of the PLX3397 treatment. In the open field test, we could not detect any difference between groups in the distance traveled (Fig. 3B; 29.2 ± 2.3 m vs. 26.8 ± 1.2 m; *t-test*, $p = 0.38$), whereas mice from the control group spent slightly more time in the periphery (505 ± 10 s vs. 480 ± 11 s; *U test*, $p = 0.043$). In the novel object location task (NOLT), PLX-treated animals spent significantly more time exploring the displaced objects compared to age-matched controls (Fig. 3C; discrimination ratio: 9.46 ± 6.5 % vs. 28.87 ± 5.9 %; *t-test*, $p = 0.043$). In the novel object recognition task (NORT), mice from both groups spent a significant amount of time exploring the new objects, i.e. behaved like young mice, and we could not detect any differences in the discrimination ratio between both groups (Fig. 3D; 27.79 ± 10.9 % vs. 25.36 ± 9.6 %; *t-test*, $p = 0.86$).

In the more cognitively challenging Labyrinth task (dry maze), resambling Morris water maze, mice use egocentric and allocentric spatial navigation strategies to reach a reward (Fig. 3E). Here, in comparison to the Morris water maze, one can avoid a stress and quantify the numbers of errors made which is an ideal metric to estimate memory performance in mice (Maei et al., 2009). However, mice in both groups showed good learning, and we found no differences in spatial memory acquisition and probe tests between groups in the latency to reward (Fig. 3F), or the number of errors made (Fig. 3G).

These data suggest that the mild microglia reduction after PLX treatment rescued impaired hippocampus-dependent memory in NOLT in aged mice but did not affect performance in NORT and dry maze, in which both control and PLX-treated aged mice performed quite well.

3.5. PLX treatment enhances synaptic plasticity in aged mice

Next, to test whether the microglial changes in PLX-treated mice impact basal synaptic transmission and synaptic plasticity in the aging brain, we performed extracellular recordings in CA3-CA1 synapses in transverse hippocampal slices. Input-output characteristics of fEPSPs in PLX-treated and control groups were plotted for different stimulus intensities, and no treatment effect was detected (Fig. 4A; *two-way RM ANOVA*, $p = 0.99$). The comparison of the paired-pulse facilitation (PPF) ratio in different stimulus intervals, likewise, did not yield any differences (Fig. 4B; *two-way RM-ANOVA*, $p = 0.35$), suggesting no effects of PLX on this form of short-term plasticity in the efficacy of transmitter release. Lastly, LTP was induced using theta-burst stimulation (TBS) and was higher in PLX-treated mice in comparison to the control group (Fig. 4C; % above the baseline level during the last 10 min of 60-min recordings: 22.81 ± 4.71 % vs. 39.16 ± 5.67 %; *t-test*, $p = 0.039$). That indicates that targeting microglia in the aging brain may be instrumental in improving synaptic plasticity.

3.6. PNN numbers and composition

PLX treatment did not change the overall number of either PV+ interneurons (Fig. 5A, B; 64.09 ± 4.3 per mm^2 vs. 63.02 ± 4.7 per mm^2; *U test*, $p = 0.83$) or WFA+ perineuronal nets (58.89 ± 3.7 per mm^2 vs. 52.43 ± 2.9 per mm^2; *U test*, $p = 0.16$) in the CA1 of aged mice. That

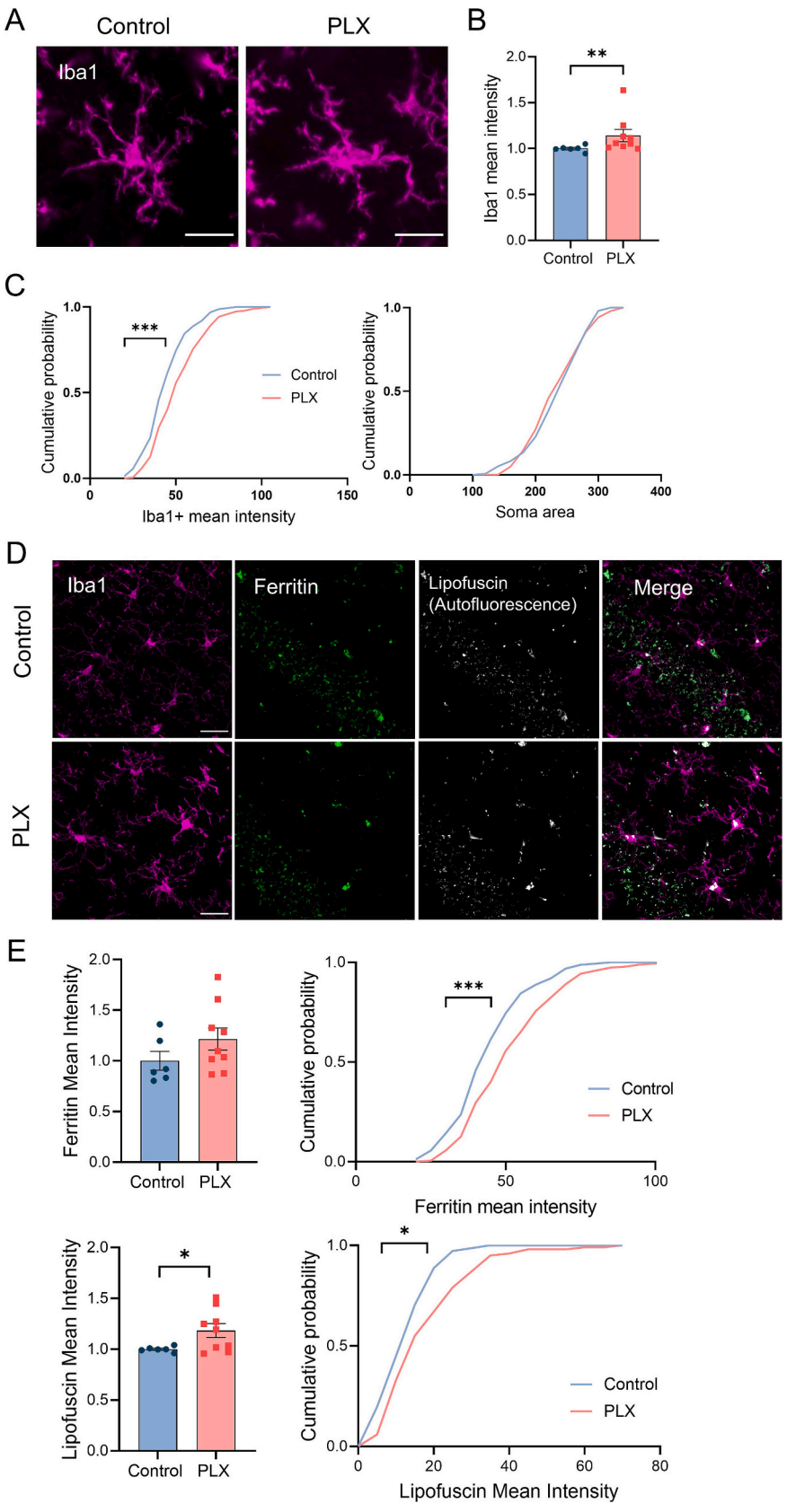

(caption on next page)

Fig. 2. PLX treatment elevates the expression of microglia markers. (A) Representative images of single Iba1+ cells used for morphological analysis. (B) Iba1 mean intensity is higher in PLX-treated animals. (C) Cumulative frequency distributions show that the Iba1 intensity but not the soma area is changed after PLX treatment. (D) 40× images of the hippocampal CA1 with Iba1+ cells (magenta) and ferritin (green), as well as autofluorescent signal (lipofuscin, grey) as markers of cell senescence. (E) The remaining microglia express higher levels of ferritin and show greater lipofuscin signal. The scale bar is 10 μm. Bar graphs show mean ± SEM values. *p < 0.05, ** p < 0.01, ****p < 0.0001; t-test, n = 6–9 mice per group. Cumulative probability curves reflect data from all analyzed microglia cells ($n = 71$ microglia cells from 6 control mice and 100 cells from 9 PLX-treated mice). (For interpretation of the references to colour in this figure legend, the reader is referred to the web version of this article.)

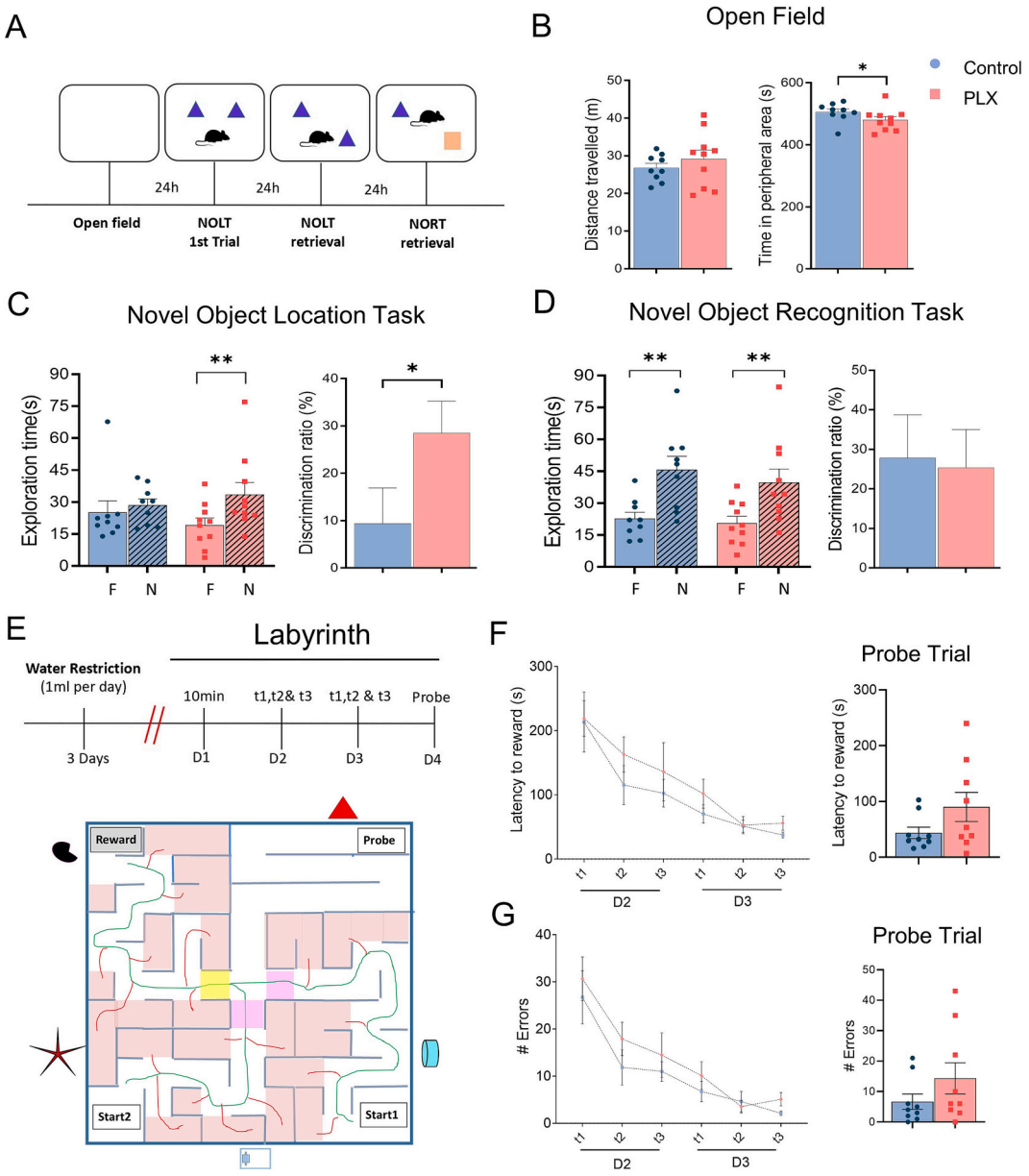

Fig. 3. PLX treatment improves cognitive performance in aged mice. (A) Hippocampus-dependent memory functions were tested in 25- to 26-month-old mice with and without PLX treatment. (A) Timeline of experiments, including details of cognitive tests. (B) Both groups of aged mice traveled a similar distance in the open field. Mice from the control group spent slightly more time in the periphery. (C) In the novel object location test (NOLT), mice explored the familiar (F) and novel (N) locations of objects. PLX-treated aged mice spent more time exploring the displaced objects than age-matched controls. (D) In the novel object recognition test (NORT), animals from both groups were able to discriminate between old (F) and novel (N) objects. (E) Timeline and design of dry maze (Labyrinth) experiments. (F & G) However, analysis of the spatial learning and memory using the dry maze (Labyrinth) did not show any difference in terms of the latency to reward (H), the number of errors made (I), and the distance traveled to the target (J). Bar graphs show mean ± SEM values. *p < 0.05, **p < 0.01, ***$p < 0.001$ and **** p < 0.0001 represent significant differences between aged vehicle ($n = 9$) and aged PLX (n = 9) mice.

finding aligns with previous studies using PLX (Strackeljan et al., 2021; Barahona et al., 2022). Additionally, there were no changes in the intensities of PV (1 ± 0.03 vs. 1.07 ± 0.09; *W's t-test*, $p = 0.5$; Fig. 5B), WFA (1 ± 0.03 vs. 1.01 ± 0.07; *Wel's t-test*, $p = 0.88$; Fig. 5B), aggrecan (1 ± 0.13 vs. 1.26 ± 0.12; *t-test*, $p = 0.21$; Fig. S3) and neurocan (1 ± 0.06 vs. 1.08 ± 0.10; *t-test*, $p = 0.57$; Fig. S3).

The results of the PNN unit analysis of the fine structural organization of PNNs were similar to what we previously observed in young

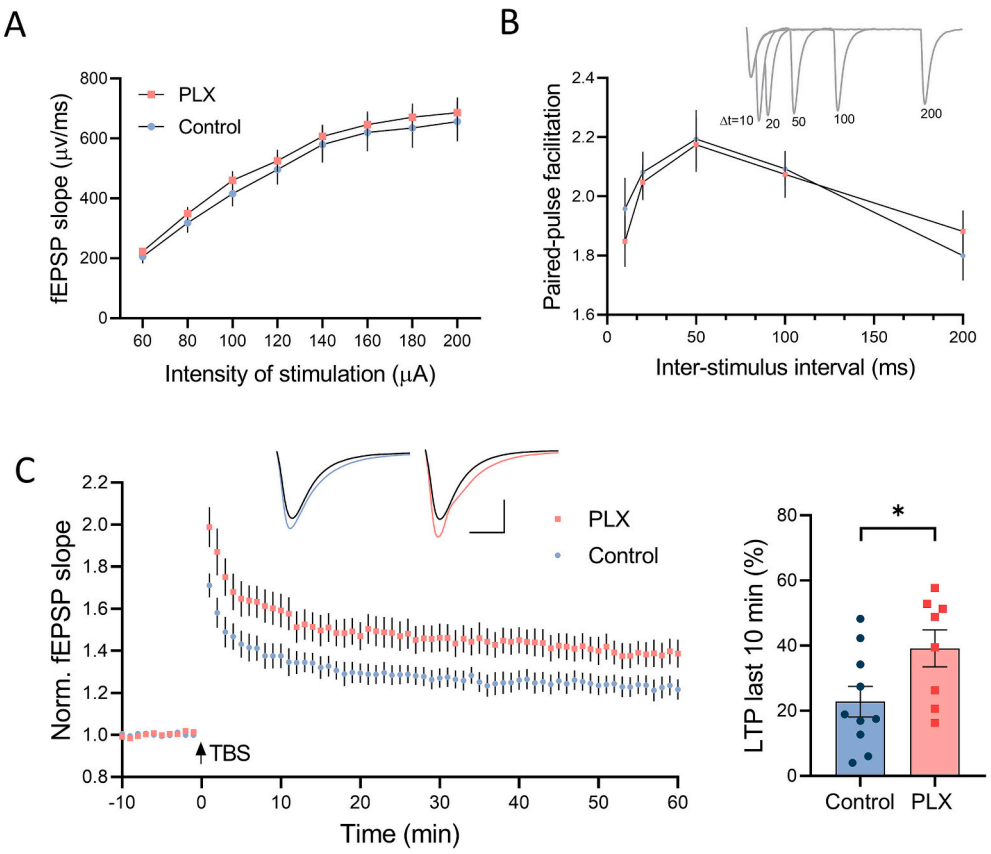

Fig. 4. PLX treatment enhances synaptic plasticity in aged mice. (A) Input-output curves of fEPSP's slope versus stimulus intensity at the CA3-CA1 synapses from control and PLX-treated groups. (B) Comparison of PPF ratio in slices from control and PLX-treated group in different time intervals. Scale bars, 0.5 mV and 20 ms. (C) Left, the time course of LTP following TBS. The mean slope of fEPSPs recorded 0–10 min before TBS was set to 1. The arrow marks the time of TBS administration. Right, a significant difference among the groups was detected for the last 10 min of recordings. Scale bars: 0.5 mV and 10 ms. Bar graphs show mean ± SEM values. *p < 0.05, t-test, $n = 10$ slices from 4 control mice and 8 slices from 4 PLX-treated mice.

animals (Strackeljan et al., 2021). After microglia reduction, the holes of single PNN units were slightly smaller (2.35 ± 0.03 vs. 2.21 ± 0.03; *KS-test*, $p < 0.0001$), and the intensity of ECM signal at the "border" around the holes was higher (Fig. 5C, D; 95.75 ± 1.2 vs. 102.6 ± 1.3; *KS-test*, $p = 0.001$), meaning that more ECM may be associated with synapses located in PNN holes.

3.7. Microglia reduction increases brevican in perisynaptic ECM in CA1 stratum radiatum but not as part of PNNs

Our previous study in young adult animals revealed that complete microglia depletion leads to an increase in brevican around excitatory synapses in the *stratum radiatum* but not in the *stratum oriens* of the CA1 region (Strackeljan et al., 2021). Similarly, in this current study, we observed that PLX treatment in aged mice increased the intensity of brevican around excitatory presynaptic terminals in the *stratum radiatum* (Fig. 6A, B, C; 1 ± 0.05 vs. 1.25 ± 0.04; *t-test*, $p = 0.002$), but not in the *stratum oriens* (1 ± 0.05 vs. 1.15 ± 0.06; t-test, $p = 0.1$; Fig. S4). The mean intensity of brevican integrated in PNNs in the hippocampal CA1 remains unchanged (1 ± 0.03 vs. 1.03 ± 0.06; *t-test*, $p = 0.66$; Fig. S3).

3.8. Changes in pre- and postsynaptic markers in CA1 stratum radiatum

Next, we analyzed the effects of PLX treatment on pre- (vGlut1) and postsynaptic (PSD-95) markers of excitatory synapses and inhibitory presynaptic marker vGAT in the CA1 area to identify synaptic correlates of the NOLT memory and LTP enhancement observed in aged mice treated with PLX. We could not detect any changes in the mean vGluT1 intensity per ROI (*stratum oriens*: 1 ± 0.06 vs. 0.9 ± 0.04; *t*-test, $p = 0.89$; *stratum radiatum*: 1 ± 0.06 vs. 1.04 ± 0.03; *t*-test; $p = 0.54$), density of vGluT1 puncta (*stratum oriens*: 40.6 ± 1.7 /100 μm^2 vs. 41.6 ± 1.3 /100 μm^2; t-test, $p = 0.6$; *stratum radiatum*: 40.7 ± 1.8 /100 μm^2 vs. 41.1 ± 1.3 /100 μm^2; t-test, $p = 0.88$) or size of puncta (*stratum oriens*: 0.317 ± 0.008 μm^2 vs. 0.315 ± 0.007 μm^2; t-test, $p = 0.82$; *stratum radiatum*: 0.32 ± 0.01 vs. 0.322 ± 0.01 μm^2; *t*-test, $p = 0.88$. However, we detected a higher single vGluT1 puncta intensity after PLX treatment using the analysis of cumulative frequency distributions (Fig. 6C; 1 ± 0.006 vs. 1.095 ± 0.006; KS-test, $p < 0.0001$).

At the postsynaptic level, we also observed slight changes in the distribution of PSD-95 intensity in the CA1 *stratum radiatum* (Fig. 6D, E; 1 ± 0.002 vs. 1.018± 0.002; KS-test, p < 0.0001) after PLX treatment. However, there was no clear shift of distribution to the right as was seen for vGluT1 and brevican, but a narrower peak and longer tails in the distribution of PSD-95 intensity after PLX treatment.

Analysis of GABAergic synapses after PLX treatment revealed an increase in the intensity of vGAT immunostaining of presynaptic puncta in *stratum radiatum* (1.0 ± 0.08 vs. 1.34 ± 0.09; *t-test*; $p = 0.024$) without any changes in the area and density of these puncta (Fig. 6F, G; area: 0.43 ± 0.02 μm^2 vs. 0.44 ± 0.01 μm^2; t-test, $p = 0.45$; density: 19.6 ± 1.05 /100 μm^2 vs. 22.3 ± 1.17 /100 μm^2; Welch's test, $p = 0.13$).

3.9. Microglia reduction leads to downregulation of C1q in CA1 stratum radiatum

Microglia are the primary source of the complement factor C1q, a protein involved in synaptic pruning (Fonseca et al., 2017; Hong et al., 2016). Here, we revealed that PLX treatment led to a prominent reduction in C1q immunofluorescence in the CA1 *stratum radiatum* (1.0

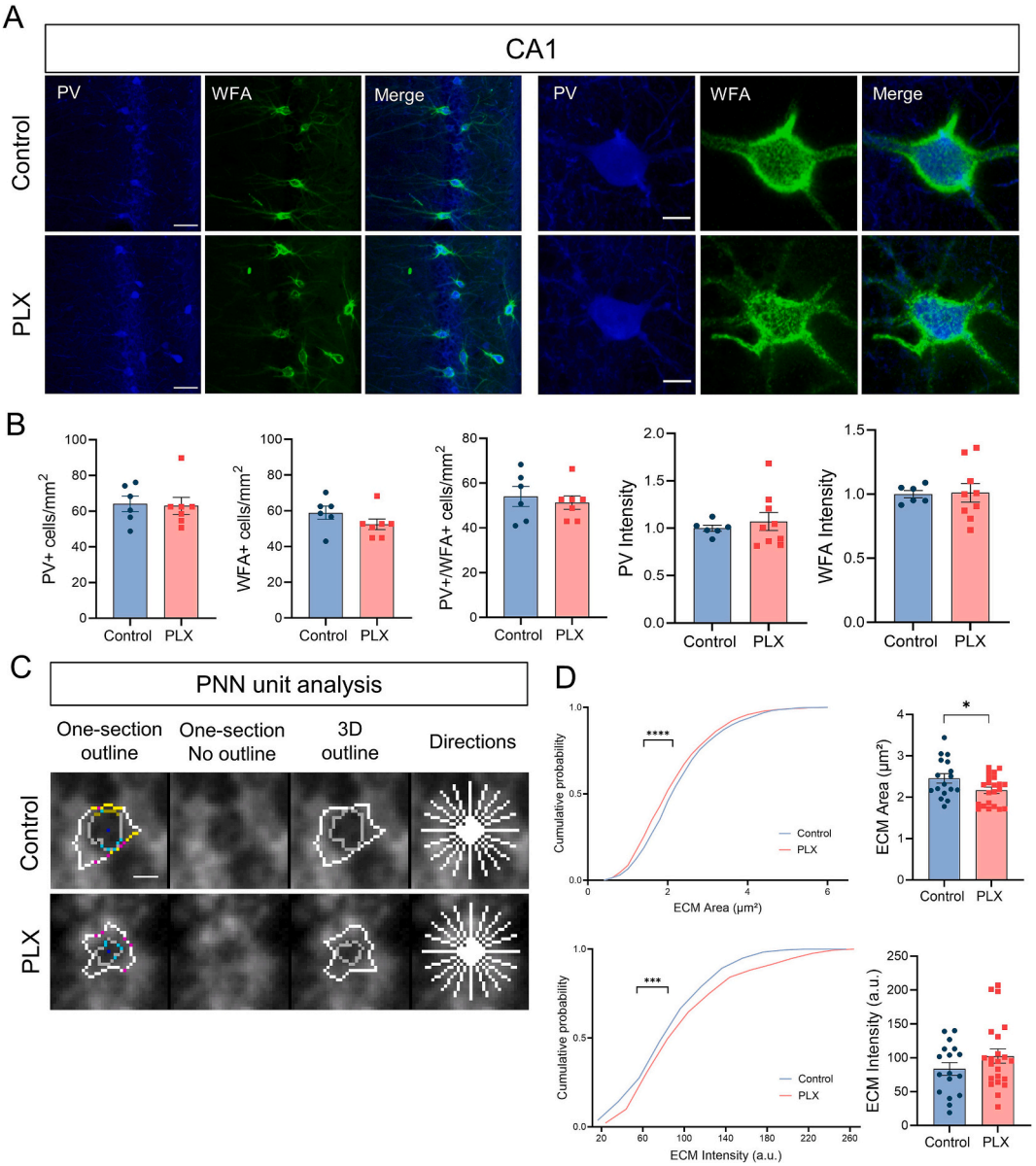

Fig. 5. PLX treatment induces changes in PNN holes and surrounding ECM. (A) Representative 20× and 63× images of PV+ cells (blue) and their surrounding PNNs (green) in the CA1. (B) PLX treatment does not change the number of PV+ or PNN+ cells or their intensity. (C) Fine structure analysis of single PNN holes in a single *Z*-plane (one-section) and 3 Z-planes (3D). The 20 tracking directions used to calculate the PNN units are displayed on the far right. Grey lines represent the outline of the PNN holes, white lines represent the outer ECM barrier, the magenta dots are positions of global maxima per direction used to compute the outer barrier, the cyan dots represent the first pixels above the set threshold to compute hole outline. (D) The cumulative distribution functions show smaller PNN holes with more intense ECM after microglia reduction. Scale bars: 50 µm (A, left panel), 10 µm (A, right panel) and 1 µm in C. Bar graphs show mean ± SEM values. *p < 0.05, ** p < 0.01, ****p < 0.0001; t-test or KS-test; data from n = 6–9 animals in each group for global PV and WFA analysis (B). For fine structure analysis, 17 cells from 5 control animals and 22 cells from 7 PLX-treated mice were included (D). (For interpretation of the references to colour in this figure legend, the reader is referred to the web version of this article.)

± 0.15 vs. 0.29 ± 0.1; *t-test*, $p = 0.0014$) but not in *stratum oriens* (1.0 ± 0.18 vs. 1.0 ± 0.06; *U test*, $p = 0.21$) (Fig. 7). However, the expression levels of CD68, a lysosomal protein enriched in active phagocytic microglia, and the expression of microglial TREM2, which is known to have anti-inflammatory properties, were not altered by PLX treatment (Fig. 7), pointing to rather specific changes in the microglial activity towards synapses.

4. Discussion

In this study, we investigated the effects of pharmacological inhibition of CSF1R on alleviating various age-associated hippocampal abnormalities. Strikingly, we found the enhancement of hippocampus-dependent cognitive function and synaptic plasticity in the aged mice treated with PLX. Moreover, this treatment increased the expression of presynaptic markers of glutamatergic and GABAergic synapses vGluT1 and vGAT, and perisynaptic brevican, previously reported to influence excitatory synaptic transmission. These changes were specifically detected in the CA1 *stratum radiatum* but not in *str. oriens*, correlating with a layer-specific reduction in the complement protein C1q that tags synapses for synaptic modifications by microglia. The observed prominent reduction in C1q (70 %) is much higher than the modest reduction in microglial density in the CA1 region (14 %), arguing that the major cause of C1q alterations is changes the state of microglia due to PLX

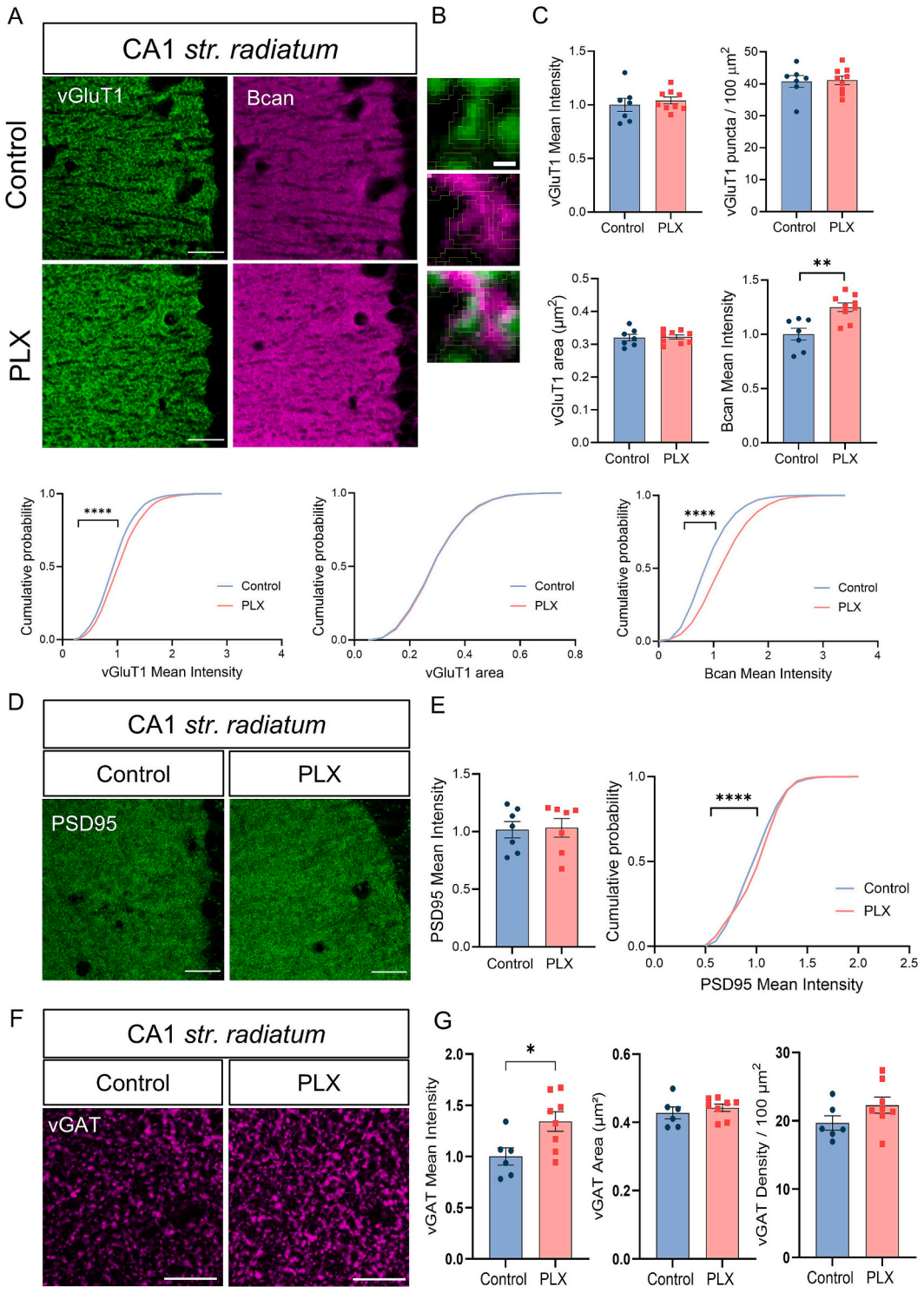

Fig. 6. Increased perisynaptic brevican around excitatory presynaptic terminals. (A) Representative 63× images of CA1 *stratum radiatum* in the aged brain. (B) Zoomed image of presynaptic vGluT1+ puncta (green) with surrounding brevican (magenta). (C) Analysis of vGluT1 and brevican after PLX treatment shows an increase in the intensity of vGluT1 and perisynaptic brevican in *stratum radiatum*. (D) 63× images of PSD-95 puncta in *stratum radiatum*. (E) Quantifications of PSD-95 in the corresponding area show changes in the distribution, which are indicative of changes in PSD-95 variability. Scale bars: 20 µm (A, D) and 1 µm (B). Bar graphs show mean ± SEM values per mouse. *p < 0.05, ** p < 0.01, ****p < 0.0001; t-test or KS-test. Cumulative probability curves reflect data from all analyzed puncta (n = 3271 puncta from 7 control mice and 4311 puncta from 9 PLX-treated mice). (F) Representative 63× images of CA1 *stratum radiatum* with vGAT puncta (magenta). (G) Analysis of vGAT+ puncta after PLX treatment shows an increase in the intensity of vGAT staining in *stratum radiatum* (1.0 ± 0.08 vs. 1.34 ± 0.09; *t-test*; p = 0.024). Scale bars: 15 µm. Bar graphs show mean ± SEM values. *p < 0.05, ** p < 0.01, ****p < 0.0001. (For interpretation of the references to colour in this figure legend, the reader is referred to the web version of this article.)

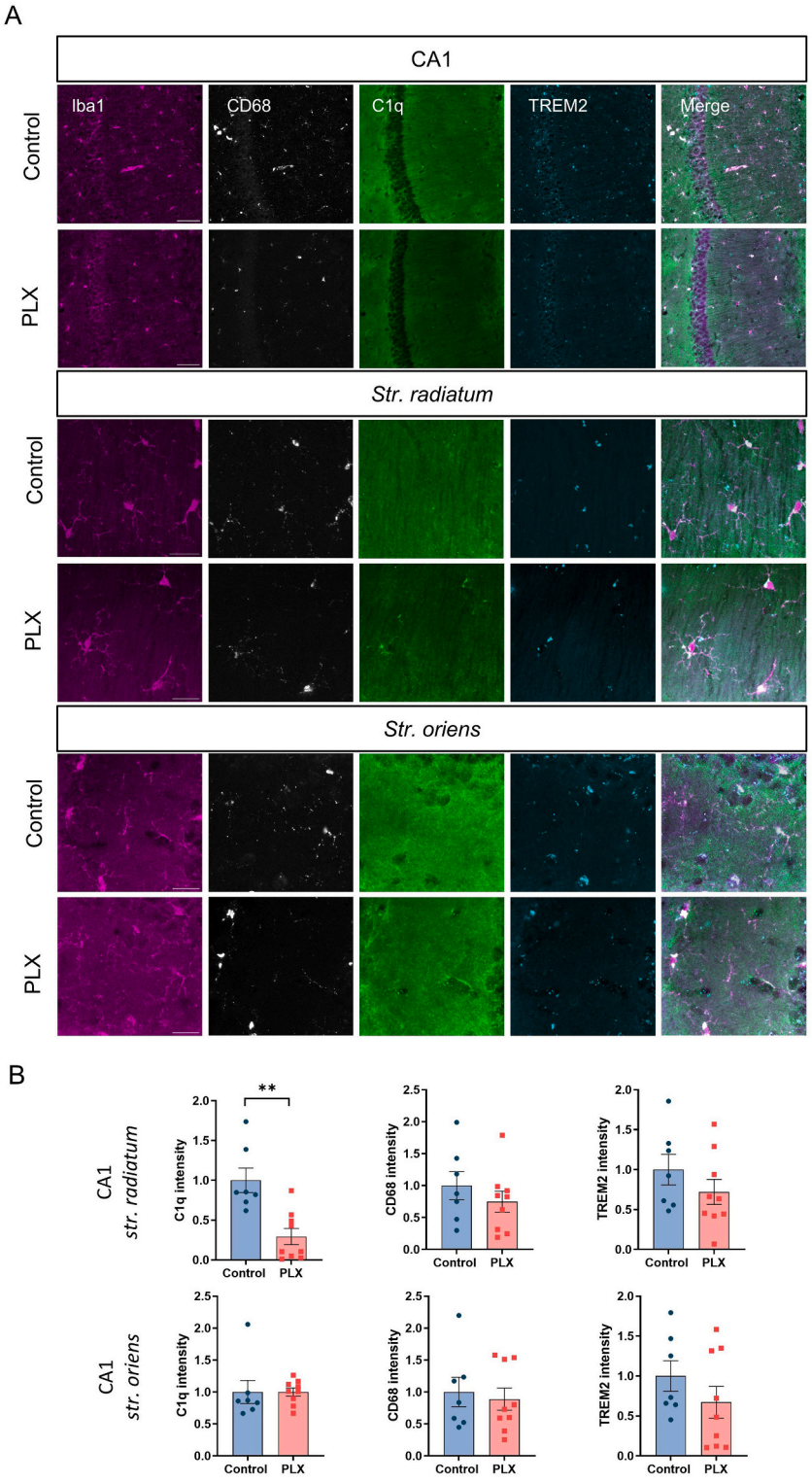

Fig. 7. PLX treatment decreases the expression of C1q in the aged hippocampus. (A) Representative 40× images of Iba1 (magenta), CD68 (grey), C1q (green) and TREM2 (cyan) in the hippocampal CA1. (B) The reduction in microglia density leads to a specific decrease in the C1q expression in CA1 *stratum radiatum* but does not occur in *stratum oriens*. The TREM2 expression inside microglial soma was not altered. Scale bar is 50 μm for CA1 and 20 μm for *stratum radiatum* and *stratum oriens.* Bar graphs show mean ± SEM values. *p < 0.05, ** p < 0.01, ****p < 0.0001; t-test, n = 6–9 mice per group. (For interpretation of the references to colour in this figure legend, the reader is referred to the web version of this article.)

treatment. This is in line with a lack of significant correlation between C1q levels and microglial density in the CA1 region at the individual animal level (Spearman coefficient of correlation = 0.098, $p = 0.729$).

Several previous works have studied the effects of alterations in microglia numbers in the brains of young and aged mice. The inhibition of CSF1R is known to deplete up to 99 % of CNS microglia, although they rapidly repopulate after the termination of treatment (Elmore et al., 2014; Huang et al., 2018; Elmore et al., 2015). The degree of microglia

reduction depends on the type of CSF1R inhibitor used, the length of the treatment and the concentration. Considering the risks of infection, one critical question is whether prominent microglia depletion without repopulation is clinically friendly to CNS functions in aged humans. Moreover, the complete inhibition of the CSF1R may result in the premature death of mice in adulthood (Ginhoux et al., 2010; Erblich et al., 2011), indicating the survival of mice beyond adulthood critically depends on the presence of microglia. Therefore, it is reasonable to study the effects of PLX3397 at concentrations that do not deplete microglia but rather modestly reduce the number of microglial cells as done in the present work (i.e., by 14 %, 27 %, and 25 % in the CA1, DG, and RSC, respectively, after 28 days of treatment), bringing microglia numbers back to the level of young controls. A study by Bennet and co-workers showed partial microglia depletion in 15-month-old Tg4510 mice after PLX3397 (Bennett et al., 2018). There seem to be age-related differences in the response of microglia to PLX3397 treatment. In a study by Yegla and colleagues, the number of Iba1+ cells was significantly higher in the aged compared to young controls (Yegla et al., 2021). Contrary to our results, they reported that partial microglia depletion led to impaired synaptic and cognitive function in aged rats. In another study, mice received either a low (300 mg/kg) or high (1200 mg/kg) dose of PLX5622 for 7 days. Notably, both doses significantly reduced microglial cells in the motor cortex. Young mice showed 44 % and 84.4 % reductions for low and high doses, respectively. Similarly, aged mice experienced reductions of 32 % and 80 % (Stojiljkovic et al., 2022). However, the effects on synaptic plasticity and cognition were not elucidated. Another recent study investigating the impact of a 7-day treatment with PLX5622, which resulted in 89 % microglial depletion in aged mice, and suggested that microglial depletion followed by repopulation promotes spatial learning and memory and LTP (Elmore et al., 2018). Similarly, our study highlights the beneficial effects of PLX treatment in aged mice. By avoiding microglia depletion, we demonstrate a more clinically friendly alternative with similar positive effects. Thus, we show that microglia repopulation is not the unique approach to obtaining synaptic and cognitive improvements in the aging brain.

One limitation of our study is that we cannot entirely rule out the possibility of unintended side effects of the treatment regarding the peripheral immune system. It is known that PLX3397 also targets peripheral immune cells, even though research has shown that the impact on macrophages in healthy wild-type mice is moderate (Mok et al., 2014). Despite this, upon aging, a disruption of the integrity of the blood-brain-barrier leads to the infiltration of immune cells into the brain, contributing to the inflammatory state. Keeping this in mind, the positive effect of CSF1R inhibition on cognition and synaptic plasticity in aged mice could at least partially be due to the targeting of peripheral immune cells.

After depleting 14 % of microglia in the CA1 of aged mice, the resident microglial population had slightly modified structural features. One such feature is the increase in Iba1 expression without any gross alteration in the degree of activation, as we observed no differences in the somatic area (Chan et al., 2018; Shaerzadeh et al., 2020) and no differences in many parameters characterizing microglial arborizations, except for the maximal branch length that was slightly reduced after PLX treatment. Further analysis revealed modestly increased ferritin immunoreactivity and lipofuscin signal in the remaining microglia after PLX treatment. Ferritin is a commonly used protein marker for senescent microglia in mice and human tissues (Lopes et al., 2008; Streit et al., 2004; Zhang et al., 2014). The level of lipofuscin autofluorescence increases with aging (Burns et al., 2020) and ferritin is known to bind to iron and regulate the iron content in the brain (Streit et al., 2004; Zhang et al., 2014). The senescent microglia show deficits in phagocytosis (Ye et al., 2017), in line with the reduced expression of C1q found in the present study.

A change in the microglial state may also lead to altered interaction between microglia and other glial cells. The current data regarding the effect of CSF1R inhibition on the astrocytic marker GFAP is conflicting. While some studies state that no differences in astrocytes can be detected after PLX treatment, others report a reduction in astrogliosis (Johnson et al., 2023). However, in their original work introducing the CSF1R inhibitor PLX3397, Elmore and colleagues stated that the PLX treatment increased whole-brain levels of GFAP mRNA and protein but not the number or morphology of GFAP+ cells in brain sections, including the hippocampus and adjacent cortical area (Elmore et al., 2014). Here, we detected increased GFAP+ cell density in the retrosplenial cortex of PLX-treated mice but not in the hippocampus. It is known that astrocytes and microglia interact and pro-inflammatory cytokines released by reactive microglia may induce an inflammatory state in astrocytes (Liddelow et al., 2017). Possibly, these interactions caused an increase in GFAP number in the retrosplenial cortex. However, as we did not focus on the RSC for further analysis the underlying cause was not identified but could be addressed in future experiments.

The aged brain is highly populated by microglia in a perpetually activated state that coincides with age-related cognitive and synaptic decline (Norden et al., 2015). Additionally, activated aged microglia are partially senescent, continuously producing inflammatory cytokines and expressing the phagocytic phenotype (Mosher and Wyss-Coray, 2014; Greenwood and Brown, 2021). Aging is strongly associated with the decline in hippocampus-dependent cognitive functions in aged mice and humans. A study by Vegh and colleagues showed reduced object recognition as well as spatial learning and memory in aged mice (Yang et al., 2021; Végh et al., 2014). Studies have also shown that the depletion of microglia with repopulation, besides reducing neuroinflammation (Coleman et al., 2020), also enhances cognition and synaptic transmission in aged mice (Elmore et al., 2018). These positive effects on cognitive function seem to be limited to either repopulation experiments or to studies on animal models of pathological states, including Alzheimer's disease or brain after cranial irradiation (Dagher et al., 2015; Acharya et al., 2016). Complete microglia depletion in young and healthy animals has no beneficial effects (Elmore et al., 2014; Elmore et al., 2018; Spangenberg et al., 2019). In the present study, PLX-treated aged mice displayed enhanced long-term NOLT memory without improving performance in the NORT. These findings align with experiments conducted in 15-month-old 3xTG-AD mice where microglia reduction by 30 % improved performance in NOLT but not in NORT (Dagher et al., 2015). Regarding synaptic plasticity and transmission, the mechanisms underlying memory acquisition and storage (Martin et al., 2000), published data indicate that LTP enhancement in aged mice brains after PLX treatment relies on microglial repopulation (Elmore et al., 2018). That suggests that microglia functions in the aging brain impair synaptic plasticity. Contrarily, here we report for the first time that mild microglial depletion without repopulation can enhance LTP-dependent synaptic transmission in the hippocampus of aged mice. To better explain these findings, we investigated the effect of PLX treatment on both synaptic and synaptic pruning markers in the hippocampal CA1, aiming to identify correlates for enhancing NOLT performance and LTP. Consistent with these findings, the reduction of microglia led to the elevated intensity of vGluT1 and vGAT and changes in variability of PSD95 levels. While vGluT1 usually is reduced in the hippocampus of aged rodents and contributes to the impairment of memory formation and synaptic transmission (Canas et al., 2009; Cheng et al., 2011; Ménard et al., 2015), contradictory data has been reported about the expression of PSD-95 depending on the observed age point and brain region (Nyffeler et al., 2007; VanGuilder et al., 2011; Preissmann et al., 2012). An age-related continuous decrease in the VGAT level in the rodent hippocampus has been reported (Canas et al., 2009). Interestingly, the effects on vGluT1 were exclusive to the CA1 *stratum radiatum*, the region that contains synapses potentiated during LTP experiments and facilitates memory formation (Riebe and Hanse, 2012; Montero-Crespo et al., 2021). Alteration in the expression of vesicular transporters may affect the quantal size and, hence the efficacy of synaptic transmission (Wilson et al., 2005). Finally, we found brevican upregulated in the CA1 *stratum radiatum* after PLX treatment, similar to

what we previously reported in young animals and discussed at length (Strackeljan et al., 2021). We could confirm that microglia depletion seems to exclusively affect the brevican as part of perisynaptic neuropile in contrast to brevican in PNNs. The functional importance of this finding is underscored by the evidence that brevican plays a role in the proper function of synapses, as brevican-KO mice display impairments in LTP (Brakebusch et al., 2002). Furthermore, brevican regulates the activity of PV+ interneurons by interacting with potassium channels and glutamate receptors (Cangalaya et al., 2024). PLX-induced changes in expression of (peri)synaptic markers are in line with multiple studies demonstrating that microglia influence synaptic expression throughout the lifespan, impacting development, adulthood, aging, and disease (Li et al., 2024; Wang et al., 2020; Parkhurst et al., 2013; Stevens et al., 2007).

In our search for mechanisms underlying (peri)synaptic changes, we identified a reduced expression of the complement protein C1q after PLX treatment. Microglia are the primary source of C1q in the brain (Fonseca et al., 2017). Previous research has shown that high doses of PLX5622 (1200 mg/kg) reduce C1q levels in the hippocampus of adult mice (Chung et al., 2023). Our study suggests that even lower doses may have a similar effect. During development, the interaction between microglia and components of the complement cascade, including C1q and C3, are known to be involved in the pruning of synapses in an activity-dependent manner and, therefore, in the maturation of synaptic circuits (Stevens et al., 2007; Stephan et al., 2012; Schafer et al., 2012; Weinhard et al., 2018). A recent study shows that these mechanisms also play a part in Alzheimer's disease, where inhibiting either C1q, C3, or microglia prevents the early synapse loss characteristic of the disease pathology (Hong et al., 2016). Our time-lapse analysis directly demonstrated the elevated elimination of spines after inoculation of Tau proteins derived from Alzheimer's disease patients, with the rate of spine elimination correlating with the expression of complement proteins (Cangalaya et al., 2023). In the hippocampus of aged mice, C1q is strongly upregulated in proximity to synapses, which is associated with cognitive decline. However, aged C1q-deficient mice have similar spine numbers as wild-type controls, suggesting that C1q-mediated synapse-microglia interactions may induce synaptic modifications rather than changes in the balance in spine formation/elimination in these conditions. Microglia is releasing MPP9 and ADAMTS4, which are capable of proteolytic digestion of PNN components. Microglia may also phagocytose PNNs and C1q-C3-C3R interactions are likely to be involved in this type of ECM remodeling (Cangalaya et al., 2024). Thus, it is plausible to assume that less C1q at synapses after PLX treatment may lead to more perisynaptic ECM around synapses located in the neuropil and PNN holes, reducing the area of holes.

In conclusion, we presented novel evidence that microglia targeting by modest CSF1R inhibition in the aged brain positively influences cognitive and synaptic functions. As the changes associated with aging have significant effects on individual lives, such cognition-boosting treatment without major loss of microglia is of great practical interest. Further investigation is needed regarding microglial activity after modest CSF1R inhibition to counteract infection and aggregation of toxic peptides and proteins.

Funding

This research was supported by the DFG (362321501/RTG 2413 SynAGE, TP5, TP6, A1 and B1) to A.D., BMBF (16LW0464/Go-Bio-Initial CogniSia-2) and DZNE Stiftung (T0531/43703/2023/hhe) to C. C..

Availability of data and materials

The data supporting the findings of this study are available from the corresponding author upon request.

Ethics approval and consent to participate

All animal experiments were conducted in accordance with ethical animal research standards dened by the Directive 2010/63/EU, the German law and the recommendations of the Ethical Committee on Animal Health and Care of the State of Saxony-Anhalt, Germany (license number: 42502–2-1346).

Declaration of generative AI and AI-assisted technologies in the writing process

During the preparation of this work the authors did not use generative AI and AI-assisted technologies.

CRediT authorship contribution statement

Luisa Strackeljan: Writing – review & editing, Writing – original draft, Visualization, Methodology, Investigation, Formal analysis. **David Baidoe-Ansah:** Writing – review & editing, Visualization, Methodology, Investigation, Formal analysis. **Hadi Mirzapourdelavar:** Writing – review & editing, Validation, Methodology, Investigation, Formal analysis. **Shaobo Jia:** Writing – review & editing, Visualization, Methodology, Formal analysis. **Rahul Kaushik:** Writing – review & editing, Supervision, Resources, Methodology. **Carla Cangalaya:** Writing – review & editing, Visualization, Validation, Methodology. **Alexander Dityatev:** Writing – review & editing, Supervision, Resources, Project administration, Methodology, Funding acquisition, Conceptualization.

Declaration of competing interest

The authors declare that they have no competing interests.

Acknowledgments

We thank Constanze Seidenbecher and Renato Frischknecht from Leibniz Institute for Neurobiology for Bcan antibodies, and Katrin Boehm for technical assistance.

Appendix A. Supplementary data

Supplementary data to this article can be found online at https://doi.org/10.1016/j.expneurol.2025.115186.

Data availability

Data will be made available on request.

References

Acharya, M.M., Green, K.N., Allen, B.D., Najafi, A.R., Syage, A., Minasyan, H., et al., 2016. Elimination of microglia improves cognitive function following cranial irradiation. Sci. Rep. 6, 31545. https://doi.org/10.1038/srep31545.

Angelova, D.M., Brown, D.R., 2019. Microglia and the aging brain: are senescent microglia the key to neurodegeneration? J. Neurochem. 151, 676–688. https://doi.org/10.1111/jnc.14860.

Antunes, M., Biala, G., 2012. The novel object recognition memory: neurobiology, test procedure, and its modifications. Cogn. Process. 13, 93–110. https://doi.org/10.1007/s10339-011-0430-z.

Baidoe-Ansah, D., Sakib, S., Jia, S., Mirzapourdelavar, H., Strackeljan, L., Fischer, A., et al., 2022. Aging-associated changes in cognition, expression and epigenetic regulation of chondroitin 6-sulfotransferase Chst3. Cells. https://doi.org/10.3390/cells11132033.

Barahona, R.A., Morabito, S., Swarup, V., Green, K.N., 2022. Cortical diurnal rhythms remain intact with microglial depletion. Sci. Rep. 12, 114. https://doi.org/10.1038/s41598-021-04079-w.

Ben Abdallah, N.M.-B., Slomianka, L., Vyssotski, A.L., Lipp, H.-P., 2010. Early age-related changes in adult hippocampal neurogenesis in C57 mice. Neurobiol. Aging 31, 151–161. https://doi.org/10.1016/j.neurobiolaging.2008.03.002.

Benetatos, J., Bennett, R.E., Evans, H.T., Ellis, S.A., Hyman, B.T., Bodea, L.-G., Götz, J., 2020. PTEN activation contributes to neuronal and synaptic engulfment by microglia

in tauopathy. Acta Neuropathol. 140, 7–24. https://doi.org/10.1007/s00401-020-02151-9.
Bennett, R.E., Bryant, A., Hu, M., Robbins, A.B., Hopp, S.C., Hyman, B.T., 2018. Partial reduction of microglia does not affect tau pathology in aged mice. J. Neuroinflammation 15, 311. https://doi.org/10.1186/s12974-018-1348-5.
Bettio, L.E.B., Rajendran, L., Gil-Mohapel, J., 2017. The effects of aging in the hippocampus and cognitive decline. Neurosci. Biobehav. Rev. 79, 66–86. https://doi.org/10.1016/j.neubiorev.2017.04.030.
Bohlen und Halbach O von, Zacher C, Gass P, Unsicker K., 2006. Age-related alterations in hippocampal spines and deficiencies in spatial memory in mice. J. Neurosci. Res. 83, 525–531. https://doi.org/10.1002/jnr.20759.
Brakebusch, C., Seidenbecher, C.I., Asztely, F., Rauch, U., Matthies, H., Meyer, H., et al., 2002. Brevican-deficient mice display impaired hippocampal CA1 long-term potentiation but show no obvious deficits in learning and memory. Mol. Cell. Biol. 22, 7417–7427. https://doi.org/10.1128/MCB.22.21.7417-7427.2002.
Burns, J.C., Cotleur, B., Walther, D.M., Bajrami, B., Rubino, S.J., Wei, R., et al., 2020. Differential accumulation of storage bodies with aging defines discrete subsets of microglia in the healthy brain. Elife. https://doi.org/10.7554/eLife.57495.
Canas, P.M., Duarte, J.M.N., Rodrigues, R.J., Köfalvi, A., Cunha, R.A., 2009. Modification upon aging of the density of presynaptic modulation systems in the hippocampus. Neurobiol. Aging 30, 1877–1884. https://doi.org/10.1016/j.neurobiolaging.2008.01.003.
Cangalaya, C., Wegmann, S., Sun, W., Diez, L., Gottfried, A., Richter, K., et al., 2023. Real-time mechanisms of exacerbated synaptic remodeling by microglia in acute models of systemic inflammation and tauopathy. Brain Behav. Immun. 110, 245–259. https://doi.org/10.1016/j.bbi.2023.02.023.
Cangalaya, C., Sun, W., Stoyanov, S., Dunay, I.R., Dityatev, A., 2024. Integrity of neural extracellular matrix is required for microglia-mediated synaptic remodeling. Glia 72, 1874–1892. https://doi.org/10.1002/glia.24588.
Chan, T.E., Grossman, Y.S., Bloss, E.B., Janssen, W.G., Lou, W., McEwen, B.S., et al., 2018. Cell-type specific changes in glial morphology and glucocorticoid expression during stress and aging in the medial prefrontal cortex. Front. Aging Neurosci. 10, 146. https://doi.org/10.3389/fnagi.2018.00146.
Chelini, G., Mirzapourdelavar, H., Durning, P., Baidoe-Ansah, D., Sethi, M.K., O'Donovan, S.M., et al., 2024. Focal clusters of peri-synaptic matrix contribute to activity-dependent plasticity and memory in mice. Cell Rep. 43, 114112. https://doi.org/10.1016/j.celrep.2024.114112.
Cheng, X.-R., Yang, Y., Zhou, W.-X., Zhang, Y.-X., 2011. Expression of VGLUTs contributes to degeneration and acquisition of learning and memory. Neurobiol. Learn. Mem. 95, 361–375. https://doi.org/10.1016/j.nlm.2011.01.010.
Chung, H.-Y., Wickel, J., Hahn, N., Mein, N., Schwarzbrunn, M., Koch, P., et al., 2023. Microglia mediate neurocognitive deficits by eliminating C1q-tagged synapses in sepsis-associated encephalopathy. Sci. Adv. 9, eabq7806. https://doi.org/10.1126/sciadv.abq7806.
Coleman, L.G., Zou, J., Crews, F.T., 2020. Microglial depletion and repopulation in brain slice culture normalizes sensitized proinflammatory signaling. J. Neuroinflammation 17, 27. https://doi.org/10.1186/s12974-019-1678-y.
Crapser, J.D., Ochaba, J., Soni, N., Reidling, J.C., Thompson, L.M., Green, K.N., 2020. Microglial depletion prevents extracellular matrix changes and striatal volume reduction in a model of Huntington's disease. Brain 143, 266–288. https://doi.org/10.1093/brain/awz363.
Dagher, N.N., Najafi, A.R., Kayala, K.M.N., Elmore, M.R.P., White, T.E., Medeiros, R., et al., 2015. Colony-stimulating factor 1 receptor inhibition prevents microglial plaque association and improves cognition in 3xTg-AD mice. J. Neuroinflammation 12, 139. https://doi.org/10.1186/s12974-015-0366-9.
Damani, M.R., Zhao, L., Fontainhas, A.M., Amaral, J., Fariss, R.N., Wong, W.T., 2011. Age-related alterations in the dynamic behavior of microglia. Aging Cell 10, 263–276. https://doi.org/10.1111/j.1474-9726.2010.00660.x.
Deng, W., Aimone, J.B., Gage, F.H., 2010. New neurons and new memories: how does adult hippocampal neurogenesis affect learning and memory? Nat. Rev. Neurosci. 11, 339–350. https://doi.org/10.1038/nrn2822.
Dityatev, A., Schachner, M., Sonderegger, P., 2010. The dual role of the extracellular matrix in synaptic plasticity and homeostasis. Nat. Rev. Neurosci. 11, 735–746. https://doi.org/10.1038/nrn2898.
Elmore, M.R.P., Najafi, A.R., Koike, M.A., Dagher, N.N., Spangenberg, E.E., Rice, R.A., et al., 2014. Colony-stimulating factor 1 receptor signaling is necessary for microglia viability, unmasking a microglia progenitor cell in the adult brain. Neuron 82, 380–397. https://doi.org/10.1016/j.neuron.2014.02.040.
Elmore, M.R.P., Lee, R.J., West, B.L., Green, K.N., 2015. Characterizing newly repopulated microglia in the adult mouse: impacts on animal behavior, cell morphology, and neuroinflammation. PLoS ONE 10, e0122912. https://doi.org/10.1371/journal.pone.0122912.
Elmore, M.R.P., Hohsfield, L.A., Kramár, E.A., Soreq, L., Lee, R.J., Pham, S.T., et al., 2018. Replacement of microglia in the aged brain reverses cognitive, synaptic, and neuronal deficits in mice. Aging Cell 17, e12832. https://doi.org/10.1111/acel.12832.
Erblich, B., Zhu, L., Etgen, A.M., Dobrenis, K., Pollard, J.W., 2011. Absence of colony stimulation factor-1 receptor results in loss of microglia, disrupted brain development and olfactory deficits. PLoS ONE 6, e26317. https://doi.org/10.1371/journal.pone.0026317.
Fonseca, M.I., Chu, S.-H., Hernandez, M.X., Fang, M.J., Modarresi, L., Selvan, P., et al., 2017. Cell-specific deletion of C1qa identifies microglia as the dominant source of C1q in mouse brain. J. Neuroinflammation 14, 48. https://doi.org/10.1186/s12974-017-0814-9.
Fu, Y., Yu, Y., Paxinos, G., Watson, C., Rusznák, Z., 2015. Aging-dependent changes in the cellular composition of the mouse brain and spinal cord. Neuroscience 290, 406–420. https://doi.org/10.1016/j.neuroscience.2015.01.039.
Gil-Mohapel, J., Brocardo, P.S., Choquette, W., Gothard, R., Simpson, J.M., Christie, B.R., 2013. Hippocampal neurogenesis levels predict WATERMAZE search strategies in the aging brain. PLoS ONE 8, e75125. https://doi.org/10.1371/journal.pone.0075125.
Ginhoux, F., Greter, M., Leboeuf, M., Nandi, S., See, P., Gokhan, S., et al., 2010. Fate mapping analysis reveals that adult microglia derive from primitive macrophages. Science 330, 841–845. https://doi.org/10.1126/science.1194637.
Green, T.R.F., Murphy, S.M., Rowe, R.K., 2022. Comparisons of quantitative approaches for assessing microglial morphology reveal inconsistencies, ecological fallacy, and a need for standardization. Sci. Rep. 12, 18196. https://doi.org/10.1038/s41598-022-23091-2.
Greenwood, E.K., Brown, D.R., 2021. Senescent microglia: the key to the ageing brain? Int. J. Mol. Sci. https://doi.org/10.3390/ijms22094402.
Gulen, M.F., Samson, N., Keller, A., Schwabenland, M., Liu, C., Glück, S., et al., 2023. cGAS-STING drives ageing-related inflammation and neurodegeneration. Nature 620, 374–380. https://doi.org/10.1038/s41586-023-06373-1.
Harrison, S.J., Feldman, J., 2009. Perceptual comparison of features within and between objects: a new look. Vis. Res. 49, 2790–2799. https://doi.org/10.1016/j.visres.2009.08.014.
Hölter, S.M., Einicke, J., Sperling, B., Zimprich, A., Garrett, L., Fuchs, H., et al., 2015. Tests for anxiety-related behavior in mice. Curr. Protoc. Mouse Biol. 5, 291–309. https://doi.org/10.1002/9780470942390.mo150010.
Hong, S., Beja-Glasser, V.F., Nfonoyim, B.M., Frouin, A., Li, S., Ramakrishnan, S., et al., 2016. Complement and microglia mediate early synapse loss in Alzheimer mouse models. Science 352, 712–716. https://doi.org/10.1126/science.aad8373.
Huang, Y., Xu, Z., Xiong, S., Sun, F., Qin, G., Hu, G., et al., 2018. Repopulated microglia are solely derived from the proliferation of residual microglia after acute depletion. Nat. Neurosci. 21, 530–540. https://doi.org/10.1038/s41593-018-0090-8.
Ianov, L., de Both, M., Chawla, M.K., Rani, A., Kennedy, A.J., Piras, I., et al., 2017. Hippocampal transcriptomic profiles: subfield vulnerability to age and cognitive impairment. Front. Aging Neurosci. 9, 383. https://doi.org/10.3389/fnagi.2017.00383.
John, N., Krügel, H., Frischknecht, R., Smalla, K.-H., Schultz, C., Kreutz, M.R., et al., 2006. Brevican-containing perineuronal nets of extracellular matrix in dissociated hippocampal primary cultures. Mol. Cell. Neurosci. 31, 774–784. https://doi.org/10.1016/j.mcn.2006.01.011.
Johnson, N.R., Yuan, P., Castillo, E., Lopez, T.P., Yue, W., Bond, A., et al., 2023. CSF1R inhibitors induce a sex-specific resilient microglial phenotype and functional rescue in a tauopathy mouse model. Nat. Commun. 14, 118. https://doi.org/10.1038/s41467-022-35753-w.
Kaushik, R., Morkovin, E., Schneeberg, J., Confettura, A.D., Kreutz, M.R., Senkov, O., Dityatev, A., 2018. Traditional Japanese herbal medicine Yokukansan targets distinct but overlapping mechanisms in aged mice and in the 5xFAD mouse model of Alzheimer's disease. Front. Aging Neurosci. 10, 411. https://doi.org/10.3389/fnagi.2018.00411.
Kaushik, R., Lipachev, N., Matuszko, G., Kochneva, A., Dvoeglazova, A., Becker, A., et al., 2021. Fine structure analysis of perineuronal nets in the ketamine model of schizophrenia. Eur. J. Neurosci. 53, 3988–4004. https://doi.org/10.1111/ejn.14853.
Lang, J., Maeda, Y., Bannerman, P., Xu, J., Horiuchi, M., Pleasure, D., Guo, F., 2013. Adenomatous polyposis coli regulates oligodendroglial development. J. Neurosci. 33, 3113–3130. https://doi.org/10.1523/JNEUROSCI.3467-12.2013.
Li, S., Liu, H., Lv, P., Yao, Y., Peng, L., Xia, T., et al., 2024. Microglia mediate memory dysfunction via excitatory synaptic elimination in a fracture surgery mouse model. J. Neuroinflammation 21, 227. https://doi.org/10.1186/s12974-024-03216-2.
Liddelow, S.A., Guttenplan, K.A., Clarke, L.E., Bennett, F.C., Bohlen, C.J., Schirmer, L., et al., 2017. Neurotoxic reactive astrocytes are induced by activated microglia. Nature 541, 481–487. https://doi.org/10.1038/nature21029.
Lopes, K.O., Sparks, D.L., Streit, W.J., 2008. Microglial dystrophy in the aged and Alzheimer's disease brain is associated with ferritin immunoreactivity. Glia 56, 1048–1060. https://doi.org/10.1002/glia.20678.
Maei, H.R., Zaslavsky, K., Teixeira, C.M., Frankland, P.W., 2009. What is the Most sensitive measure of water maze probe test performance? Front. Integr. Neurosci. 3, 4. https://doi.org/10.3389/neuro.07.004.2009.
Martin, S.J., Grimwood, P.D., Morris, R.G., 2000. Synaptic plasticity and memory: an evaluation of the hypothesis. Annu. Rev. Neurosci. 23, 649–711. https://doi.org/10.1146/annurev.neuro.23.1.649.
Ménard, C., Quirion, R., Vigneault, E., Bouchard, S., Ferland, G., El Mestikawy, S., Gaudreau, P., 2015. Glutamate presynaptic vesicular transporter and postsynaptic receptor levels correlate with spatial memory status in aging rat models. Neurobiol. Aging 36, 1471–1482. https://doi.org/10.1016/j.neurobiolaging.2014.11.013.
Mok, S., Koya, R.C., Tsui, C., Xu, J., Robert, L., Wu, L., et al., 2014. Inhibition of CSF-1 receptor improves the antitumor efficacy of adoptive cell transfer immunotherapy. Cancer Res. 74, 153–161. https://doi.org/10.1158/0008-5472.CAN-13-1816.
Montero-Crespo, M., Domínguez-Álvaro, M., Alonso-Nanclares, L., DeFelipe, J., Blazquez-Llorca, L., 2021. Three-dimensional analysis of synaptic organization in the hippocampal CA1 field in Alzheimer's disease. Brain 144, 553–573. https://doi.org/10.1093/brain/awaa406.
Mosher, K.I., Wyss-Coray, T., 2014. Microglial dysfunction in brain aging and Alzheimer's disease. Biochem. Pharmacol. 88, 594–604. https://doi.org/10.1016/j.bcp.2014.01.008.

Nguyen, P.T., Dorman, L.C., Pan, S., Vainchtein, I.D., Han, R.T., Nakao-Inoue, H., et al., 2020. Microglial remodeling of the extracellular matrix promotes synapse plasticity. Cell 182, 388–403.e15. https://doi.org/10.1016/j.cell.2020.05.050.

Norden, D.M., Muccigrosso, M.M., Godbout, J.P., 2015. Microglial priming and enhanced reactivity to secondary insult in aging, and traumatic CNS injury, and neurodegenerative disease. Neuropharmacology 96, 29–41. https://doi.org/10.1016/j.neuropharm.2014.10.028.

Nyffeler, M., Zhang, W.-N., Feldon, J., Knuesel, I., 2007. Differential expression of PSD proteins in age-related spatial learning impairments. Neurobiol. Aging 28, 143–155. https://doi.org/10.1016/j.neurobiolaging.2005.11.003.

Parkhurst, C.N., Yang, G., Ninan, I., Savas, J.N., Yates, J.R., Lafaille, J.J., et al., 2013. Microglia promote learning-dependent synapse formation through brain-derived neurotrophic factor. Cell 155, 1596–1609. https://doi.org/10.1016/j.cell.2013.11.030.

Preissmann, D., Leuba, G., Savary, C., Vernay, A., Kraftsik, R., Riederer, I.M., et al., 2012. Increased postsynaptic density protein-95 expression in the frontal cortex of aged cognitively impaired rats. Exp. Biol. Med. (Maywood) 237, 1331–1340. https://doi.org/10.1258/ebm.2012.012020.

Rich, E.L., Shapiro, M.L., 2007. Prelimbic/infralimbic inactivation impairs memory for multiple task switches, but not flexible selection of familiar tasks. J. Neurosci. 27, 4747–4755. https://doi.org/10.1523/JNEUROSCI.0369-07.2007.

Richard, A.D., Tian, X.-L., El-Saadi, M.W., Lu, X.-H., 2018. Erasure of striatal chondroitin sulfate proteoglycan-associated extracellular matrix rescues aging-dependent decline of motor learning. Neurobiol. Aging 71, 61–71. https://doi.org/10.1016/j.neurobiolaging.2018.07.008.

Riebe, I., Hanse, E., 2012. Development of synaptic connectivity onto interneurons in stratum radiatum in the CA1 region of the rat hippocampus. BMC Neurosci. 13, 14. https://doi.org/10.1186/1471-2202-13-14.

Rosenzweig, E.S., Barnes, C.A., 2003. Impact of aging on hippocampal function: plasticity, network dynamics, and cognition. Prog. Neurobiol. 69, 143–179. https://doi.org/10.1016/s0301-0082(02)00126-0.

Schafer, D.P., Lehrman, E.K., Kautzman, A.G., Koyama, R., Mardinly, A.R., Yamasaki, R., et al., 2012. Microglia sculpt postnatal neural circuits in an activity and complement-dependent manner. Neuron 74, 691–705. https://doi.org/10.1016/j.neuron.2012.03.026.

Seidenbecher, C.I., Richter, K., Rauch, U., Fässler, R., Garner, C.C., Gundelfinger, E.D., 1995. Brevican, a chondroitin sulfate proteoglycan of rat brain, occurs as secreted and cell surface glycosylphosphatidylinositol-anchored isoforms. J. Biol. Chem. 270, 27206–27212. https://doi.org/10.1074/jbc.270.45.27206.

Shaerzadeh, F., Phan, L., Miller, D., Dacquel, M., Hachmeister, W., Hansen, C., et al., 2020. Microglia senescence occurs in both substantia nigra and ventral tegmental area. Glia 68, 2228–2245. https://doi.org/10.1002/glia.23834.

Shors, T.J., Miesegaes, G., Beylin, A., Zhao, M., Rydel, T., Gould, E., 2001. Neurogenesis in the adult is involved in the formation of trace memories. Nature 410, 372–376. https://doi.org/10.1038/35066584.

Sikora, E., Bielak-Zmijewska, A., Dudkowska, M., Krzystyniak, A., Mosieniak, G., Wesierska, M., Wlodarczyk, J., 2021. Cellular senescence in brain aging. Front. Aging Neurosci. 13, 646924. https://doi.org/10.3389/fnagi.2021.646924.

Spangenberg, E., Severson, P.L., Hohsfield, L.A., Crapser, J., Zhang, J., Burton, E.A., et al., 2019. Sustained microglial depletion with CSF1R inhibitor impairs parenchymal plaque development in an Alzheimer's disease model. Nat. Commun. 10, 3758. https://doi.org/10.1038/s41467-019-11674-z.

Sparkman, N.L., Johnson, R.W., 2008. Neuroinflammation associated with aging sensitizes the brain to the effects of infection or stress. Neuroimmunomodulation 15, 323–330. https://doi.org/10.1159/000156474.

Stephan, A.H., Barres, B.A., Stevens, B., 2012. The complement system: an unexpected role in synaptic pruning during development and disease. Annu. Rev. Neurosci. 35, 369–389. https://doi.org/10.1146/annurev-neuro-061010-113810.

Stevens, B., Allen, N.J., Vazquez, L.E., Howell, G.R., Christopherson, K.S., Nouri, N., et al., 2007. The classical complement cascade mediates CNS synapse elimination. Cell 131, 1164–1178. https://doi.org/10.1016/j.cell.2007.10.036.

Stojiljkovic, M.R., Schmeer, C., Witte, O.W., 2022. Pharmacological depletion of microglia leads to a dose-dependent reduction in inflammation and senescence in the aged murine brain. Neuroscience 488, 1–9. https://doi.org/10.1016/j.neuroscience.2022.02.018.

Strackeljan, L., Baczynska, E., Cangalaya, C., Baidoe-Ansah, D., Wlodarczyk, J., Kaushik, R., Dityatev, A., 2021. Microglia depletion-induced remodeling of extracellular matrix and excitatory synapses in the Hippocampus of adult mice. Cells. https://doi.org/10.3390/cells10081862.

Streit, W.J., Sammons, N.W., Kuhns, A.J., Sparks, D.L., 2004. Dystrophic microglia in the aging human brain. Glia 45, 208–212. https://doi.org/10.1002/glia.10319.

Takebayashi, H., Yoshida, S., Sugimori, M., Kosako, H., Kominami, R., Nakafuku, M., Nabeshima, Y., 2000. Dynamic expression of basic helix-loop-helix Olig family members: implication of Olig2 in neuron and oligodendrocyte differentiation and identification of a new member, Olig3. Mech. Dev. 99, 143–148. https://doi.org/10.1016/S0925-4773(00)00466-4.

Tremblay, M.-È., Zettel, M.L., Ison, J.R., Allen, P.D., Majewska, A.K., 2012. Effects of aging and sensory loss on glial cells in mouse visual and auditory cortices. Glia 60, 541–558. https://doi.org/10.1002/glia.22287.

VanGuilder, H.D., Farley, J.A., Yan, H., van Kirk, C.A., Mitschelen, M., Sonntag, W.E., Freeman, W.M., 2011. Hippocampal dysregulation of synaptic plasticity-associated proteins with age-related cognitive decline. Neurobiol. Dis. 43, 201–212. https://doi.org/10.1016/j.nbd.2011.03.012.

Vaughan, D.W., Peters, A., 1974. Neuroglial cells in the cerebral cortex of rats from young adulthood to old age: an electron microscope study. J. Neurocytol. 3, 405–429. https://doi.org/10.1007/BF01098730.

Végh, M.J., Heldring, C.M., Kamphuis, W., Hijazi, S., Timmerman, A.J., Li, K.W., et al., 2014. Reducing hippocampal extracellular matrix reverses early memory deficits in a mouse model of Alzheimer's disease. Acta Neuropathol. Commun. 2, 76. https://doi.org/10.1186/s40478-014-0076-z.

Vogel, C., Marcotte, E.M., 2012. Insights into the regulation of protein abundance from proteomic and transcriptomic analyses. Nat. Rev. Genet. 13, 227–232. https://doi.org/10.1038/nrg3185.

von Bernhardi, R., Eugenín-von Bernhardi, L., Eugenín, J., 2015. Microglial cell dysregulation in brain aging and neurodegeneration. Front. Aging Neurosci. 7, 124. https://doi.org/10.3389/fnagi.2015.00124.

Wang, C., Yue, H., Hu, Z., Shen, Y., Ma, J., Li, J., et al., 2020. Microglia mediate forgetting via complement-dependent synaptic elimination. Science 367, 688–694. https://doi.org/10.1126/science.aaz2288.

Weinhard, L., Di Bartolomei, G., Bolasco, G., Machado, P., Schieber, N.L., Neniskyte, U., et al., 2018. Microglia remodel synapses by presynaptic trogocytosis and spine head filopodia induction. Nat. Commun. 9, 1228. https://doi.org/10.1038/s41467-018-03566-5.

Wilson, N.R., Kang, J., Hueske, E.V., Leung, T., Varoqui, H., Murnick, J.G., et al., 2005. Presynaptic regulation of quantal size by the vesicular glutamate transporter VGLUT1. J. Neurosci. 25, 6221–6234. https://doi.org/10.1523/JNEUROSCI.3003-04.2005.

Yang, S., Gigout, S., Molinaro, A., Naito-Matsui, Y., Hilton, S., Foscarin, S., et al., 2021. Chondroitin 6-sulphate is required for neuroplasticity and memory in ageing. Mol. Psychiatry 26, 5658–5668. https://doi.org/10.1038/s41380-021-01208-9.

Ye, J., Jiang, Z., Chen, X., Liu, M., Li, J., Liu, N., 2017. The role of autophagy in pro-inflammatory responses of microglia activation via mitochondrial reactive oxygen species in vitro. J. Neurochem. 142, 215–230. https://doi.org/10.1111/jnc.14042.

Yegla, B., Boles, J., Kumar, A., Foster, T.C., 2021. Partial microglial depletion is associated with impaired hippocampal synaptic and cognitive function in young and aged rats. Glia 69, 1494–1514. https://doi.org/10.1002/glia.23975.

Zhang, Y., Chen, K., Sloan, S.A., Bennett, M.L., Scholze, A.R., O'Keeffe, S., et al., 2014. An RNA-sequencing transcriptome and splicing database of glia, neurons, and vascular cells of the cerebral cortex. J. Neurosci. 34, 11929–11947. https://doi.org/10.1523/JNEUROSCI.1860-14.2014.